Microenvironmental adaptations drive obesity-associated pancreatic cancer

Katherine Minjee Chung[1†], Jaffarguriqbal Singh[2,3†], Lauren Lawres[2,3†], Kimberly Judith Dorans[1†], Rebecca Robbins[1], Arjun Bhutkar[1], Ana Babic[4], Sara A. Vayrynen[4], Andressa D. Costa[4], Jonathan A. Nowak[5], Daniel T. Chang[6], Richard F. Dunne[7], Aram F. Hezel[7], Albert C. Koong[8], Joshua J. Wilhelm[9], Melena D. Bellin[9.10], Vibe Nylander[11], Anna L. Gloyn[11,12,13], Mark I. McCarthy[11,12,13], Brian M. Wolpin[4], Tyler Jacks[1,14], Charles S. Fuchs[15,16], and Mandar Deepak Muzumdar[2,3,15,16*]

Affiliations

[1] Koch Institute for Integrative Cancer Research at MIT, Cambridge, MA 02139, USA
[2] Department of Genetics, Yale University School of Medicine, New Haven, CT 06510, USA
[3] Yale Cancer Biology Institute, Yale University School of Medicine, New Haven, CT 06510, USA
[4] Department of Medical Oncology, Dana-Farber Cancer Institute, Harvard Medical School, Boston, MA, 02114, USA
[5] Department of Pathology, Brigham and Women's Hospital, Harvard Medical School, Boston, MA 02115, USA
[6] Department of Radiation Oncology, Stanford Cancer Institute, Stanford, CA 94305
[7] Division of Hematology and Oncology, Department of Medicine, Wilmot Cancer Institute, University of Rochester Medical Center, Rochester, NY 14627
[8] Department of Radiation Oncology, The University of Texas MD Anderson Cancer Center, Houston, TX 77030
[9] Schulze Diabetes Institute and Department of Surgery, University of Minnesota Medical Center, Minneapolis, MN 55454
[10] Departments of Pediatrics, University of Minnesota Medical Center, Minneapolis, MN 55454
[11] Wellcome Centre for Human Genetics, Nuffield Department of Medicine, University of Oxford, Oxford, OX3 7BN, UK
[12] Oxford Centre for Diabetes, Endocrinology and Metabolism, Radcliffe Department of Medicine, University of Oxford, Oxford, OX3 7LE, UK
[13] Oxford NIHR Biomedical Research Centre, Oxford University Hospitals Trust, Oxford, OX3 7LE, UK.
[14] Howard Hughes Medical Institute, Massachusetts Institute of Technology, Cambridge, MA 02139, USA
[15] Department of Medicine, Yale University School of Medicine, New Haven, CT 06510, USA
[16] Yale Cancer Center, Smilow Cancer Hospital, New Haven, CT 06510, USA

[*]Correspondence to: Mandar Deepak Muzumdar, mandar.muzumdar@yale.edu
[†]These authors contributed equally to this work

Obesity is a major modifiable risk factor for pancreatic ductal adenocarcinoma (PDAC), yet how obesity contributes to PDAC development is not well understood. Moreover, whether and at what point weight loss or other obesity-related interventions impact PDAC progression remains largely unexplored with important implications for prevention and treatment. Leveraging an autochthonous genetically engineered mouse model of PDAC, we demonstrate that obesity plays a stage-specific causal and reversible role in early PDAC progression. Molecular and histologic analyses reveal prominent microenvironmental alterations in tumors from obese mice, including increased inflammation and fibrosis and evidence for marked pancreatic islet cell adaptation. In particular, we identify aberrant expression of the peptide hormone cholecystokinin (CCK) in pancreatic islets in tumors as an adaptive response to obesity and show that islet CCK expression promotes oncogenic *Kras*-driven pancreatic ductal tumorigenesis. Together, these studies link obesity, changes in the local microenvironment, and tumorigenesis and implicate endocrine-exocrine signaling beyond insulin in PDAC development. Furthermore, the reversible nature of these adaptations supports the potential of anti-obesity strategies to intercept PDAC early during progression.

Pancreatic ductal adenocarcinoma (PDAC) is the third leading cause of cancer death in the United States and is expected to become the second within the next few years[1,2]. Despite the development of combination chemotherapy, novel targeted small molecules, and immunotherapies that have revolutionized the care of many other cancers, long-term survival in PDAC remains low at <10%[2,3]. In search of drug targets, genomic studies have identified frequent mutations in the proto-oncogene *KRAS*, occurring in >90% of human PDAC tumors[4,5].

Unfortunately, no effective direct KRAS inhibitors are currently in clinical use[6]. Moreover, our recent work has demonstrated that PDAC cells can survive genetic ablation of *KRAS* both *in vitro* and *in vivo*[7,8], suggesting the likelihood of resistance to the very best KRAS inhibitors. As a result, alternative paradigms beyond genetic factors need to be explored to develop novel therapeutic and preventative strategies in PDAC.

Epidemiologic studies in prospective cohorts have identified non-genetic factors that contribute to PDAC risk. In particular, body-mass index (BMI), a surrogate measure of obesity, has recurrently been shown to be associated with an increased risk of developing PDAC[9]. More recent studies have demonstrated an association between elevated pre-diagnostic BMI with more advanced disease at diagnosis and worse survival[10]. Despite these data, the mechanisms by which obesity contributes to PDAC progression remain elusive. Previous research demonstrated that high-fat diet (HFD) can promote tumor growth or cancer progression in transplant or autochthonous models of PDAC[11-16]. These studies implicated dysregulation of fatty acid or nitrogen metabolism[12,15], COX2 activation[13], and aberrations in the desmoplastic response[12,14,16] as potential mechanisms, but were limited by: 1) the slow onset of obesity and lack of rapid reversibility in HFD models; 2) variations in fat content, types of fat, and age of administration in HFD protocols, which can confound results[17]; and 3) an emphasis on transplant rather than autochthonous models that more faithfully recapitulate tumor progression and the microenvironment of the human disease[18]. Moreover, whether and at what point weight loss or other anti-obesity interventions influence PDAC progression is not known, despite significant implications for prevention and treatment[19].

To overcome these important limitations, we generated a rapid and reversible autochthonous model of obesity-associated PDAC progression. We utilized leptin-deficient (*ob/ob*) mice, which, unlike HFD models, exhibit early onset obesity due to impaired appetite suppression and decreased metabolism[20]. We crossed *ob/ob* mice with *KC* (*Pdx1-Cre; Kras*$^{LSL\text{-}G12D/WT}$) mice predisposed to the development of precursor pancreatic intraepithelial neoplasia (PanINs)[21] (**Figure 1a**). *KC; ob/ob* (*KCO*) mice were obese and developed increased primary ductal tumor burden, enhanced progression to adenocarcinoma, and markedly shortened survival compared to non-obese *KC* mice (**Figures 1b-f**). We similarly observed decreased survival with a separate obesity model induced by loss-of-function mutations in the leptin receptor (*db/db*) (**Supplementary Figures 1a,b**). Consistent with the degree of obesity, these phenotypes were significantly more severe than seen in HFD models[12,13,16]. Furthermore, while increased leptin signaling has been proposed as a mechanism by which obesity promotes tumorigenesis[22], our results confirm that obesity may drive pancreatic cancer development in a leptin-independent manner. To determine whether obesity is capable of enhancing tumor progression in other oncogenic *Kras*-driven autochthonous cancer models, we evaluated the effect of obesity (HFD-induced and leptin deficiency) on survival in lung cancer induced by the spontaneous activation of a "hit-and-run" allele of oncogenic *Kras* (*Kras*^{LA2})[23]. Unlike pancreatic cancer, human epidemiologic studies do not demonstrate an association between obesity and lung cancer[24]. Consistent with these data, while all *Kras*^{LA2} mice developed morbidity from lung tumors, neither obesity induced by HFD nor *ob/ob* genotype shortened survival in these models (**Supplementary Figures 1c-f**). Together, these results support a specific effect of obesity on *Kras*-induced pancreatic cancer progression.

We next took advantage of the capacity to rapidly reverse the *ob/ob* obesity phenotype through leptin restoration to study the effects of weight loss on PDAC progression. Weight loss due to bariatric surgery reduces overall cancer incidence, though a specific effect on PDAC prevention has not been definitively demonstrated due to the low number of incident cases in these studies[25]. We generated adeno-associated viruses (AAVs) that permit expression of green fluorescent protein (AAV-GFP) or sustained leptin secretion (AAV-Leptin) following a single intramuscular injection (**Figure 2a; Supplementary Figures 2a,b**). Similar to leptin protein replacement[20], AAV-Leptin reversed multiple phenotypes of leptin deficiency including obesity , hyperglycemia, and infertility (**Supplementary Figures 2b-d**). Remarkably, early AAV-Leptin administration (at six weeks of age following obesity onset but prior to significant tumor development) impeded tumor progression proportional to the degree of weight loss (**Figures 2b-d**). In contrast, late AAV-Leptin administration (at three months of age following advanced tumor development (**Figures 1c,d**)) induced weight loss but did not impact survival (**Supplementary Figures 2e,f**). Accordingly, several of the AAV-GFP-treated mice exhibited cancer-associated weight loss (**Supplementary Figure 2e**), a poor prognostic finding in human PDAC[26]. Moreover, recombinant leptin treatment of advanced murine PDAC cells *in vitro* induced on-target downstream STAT3 and MAPK signaling, but did not alter cell viability (**Supplementary Figures 2g,h**). Consistent with the potential of weight loss to impact tumor progression in a leptin-independent manner *in vivo*, young *KCO* mice subject to caloric restriction exhibited weight loss kinetics similar to AAV-Leptin treatment and markedly reduced tumor burden compared to ad libitum fed mice (**Figures 2e,f)**. These data support a stage-specific effect of obesity on early pancreatic cancer development and the potential to halt or to delay obesity-driven PDAC progression with weight loss.

We next sought to identify the mechanisms by which obesity contributes to pancreatic ductal tumorigenesis in this model. We postulated that obesity could induce driver mutations to promote tumorigenesis via DNA damage in the setting of enhanced oxidative stress[27]. As inactivating mutations in *Trp53*, *Cdkn2a*, and *Smad4*, the hallmark recurrently mutated tumor suppressor genes (TSGs) in human PDAC[4,5], independently accelerate oncogenic *Kras*-induced pancreatic tumor development in mice[28-31], we hypothesized that tumor progression in *KCO* mice would similarly depend on additional driver gene mutations beyond oncogenic *Kras*. In support of this hypothesis, survival of *KCO* mice was comparable to what we previously observed[31] in *KPC* mice (*Pdx1-Cre; Kras*$^{LSL\text{-}G12D/WT}$*; p53*$^{flox/WT}$ or *Pdx1-Cre; Kras*$^{LSL\text{-}G12D/WT}$*; p53*$^{LSL\text{-}R172H/WT}$) harboring heterozygous mutations in *p53* (p=0.93, log-rank test). Surprisingly, IHC for the hallmark TSGs revealed persistent protein expression, and exome sequencing confirmed the absence of inactivating point mutations in these genes (**Supplementary Figure 3; Supplementary Data Table 1**). Furthermore, recurrent pathogenic mutations in other known PDAC[4,5] or pan-cancer driver genes[32] were not observed in *KCO* tumors (**Supplementary Data Tables 2-3**). These data support the conclusion that additional driver gene mutations are not required for obesity to promote pancreatic cancer development. To determine if a similar phenomenon is evident in human tumors, we performed targeted exome sequencing and immunohistochemistry (IHC) to evaluate alterations of *KRAS*, *TP53*, *CDKN2A/p16*, and *SMAD4* in 184 human tumors with known patient BMI at diagnosis (**Supplementary Table 1**). While we observed a significant increase in *SMAD4* loss with elevated BMI (odds ratio 3.82 for BMI>30 kg/m^2 compared to BMI<25 kg/m^2), the total number of driver gene alterations per tumor, which we have previously shown predicts worse PDAC outcome[33], did not significantly differ across categories of BMI (**Supplementary Table 2**). Together, these data highlight the possibility that

obesity may function independently of driver gene alterations in both mice and humans to promote pancreatic tumorigenesis.

To elucidate these non-mutational mechanisms of PDAC progression, we performed bulk RNA-sequencing (RNA-Seq) on pancreata from obese *KCO* and non-obese *KC* and *KPC* mice exhibiting comparable levels of tumor burden (**Supplementary Data Table 4**), permitting analyses of both tumor cells and their microenvironment in cancer pathogenesis. Using Independent Component Analysis (ICA), an unsupervised blind source separation technique[7,34], we identified gene expression signatures associated with inflammation, lymphocyte receptor signaling, chemokine signaling, extracellular matrix, and fibrosis as upregulated in *KCO* compared to *KC*/*KPC* mice (**Supplementary Figure 4a-d; Supplementary Data Tables 5-6**), likely representing obesity-associated alterations in the tumor microenvironment. To determine human relevance, we ranked primary human PDAC tumors from The Cancer Genome Atlas (TCGA)[5] based on gene expression correlation to these *KCO* signatures. We classified these tumors using previously-defined molecular subtypes[4] and found the *KCO*-correlated tumors to be significantly enriched with the immunogenic subtype (**Supplementary Figure 4e**), which is associated with immune cell infiltration and consequently lower tumor cell purity[4,5]. Using CIBERSORT[35] to computationally derive immune cell subsets from our murine gene expression data, we observed *KCO* tumor infiltration with predominantly myeloid cells (macrophages, resting dendritic cells, and neutrophils) and smaller proportions of lymphocytic populations (T, B, and NK cells) (**Supplementary Figure 4f**), as has previously been observed in human and mouse PDAC[36]. These proportions did not differ based on obesity status comparing *KCO* to *KC* and *KPC* mice. In contrast, pancreata from non-tumor-bearing obese *ob/ob* mice exhibited the

presence of mostly plasma cells and resting dendritic cells with a much smaller proportion of macrophages (**Supplementary Figure 4f**), suggesting the main features of pancreatic immune cell infiltration in *KCO* mice are tumor-dependent. Finally, we confirmed abundant extracellular matrix deposition and macrophage-predominant immune cell infiltration by histologic analyses of *KCO* tumor sections (**Supplementary Figure 4g**). In accordance with prior work using HFD models[14,16], these data revealed that alterations in the fibroinflammatory microenvironment are a major feature of obesity-associated pancreatic tumors.

Given the known association of chronic pancreatic inflammation (pancreatitis) with increased human PDAC risk[3] and the capacity of obesity to establish a pro-tumorigenic inflammatory microenvironment in implanted advanced PDAC models[14,37], we postulated that this microenvironment may be driving early tumor progression in *KCO* mice. Therefore, we tested the capacity of the anti-inflammatory agent aspirin and the antidiabetic drug metformin to intercept PDAC progression in *KCO* mice. In patient cohorts, both aspirin and metformin have been shown to mitigate pancreatic cancer risk[38,39], while metformin additionally exhibits anti-fibrotic properties in non-obese murine models of pancreatic cancer and lung injury[40,41]. Surprisingly, neither aspirin nor metformin impaired tumor development in *KCO* mice (**Supplementary Figure 5)**. These data along with the absence of major alterations in the pancreatic immune cell composition in obese (*ob/ob*) mice compared to mice subject to leptin restoration (**Supplementary Figure 4f**) support the possibility that the fibroinflammatory features of *KCO* tumors may be a consequence rather than a cause of tumorigenesis. Therefore, we looked further upstream for cells or factors that could both induce a pro-inflammatory microenvironment and drive tumor development.

Previous work reported that this inflammatory stimulus may derive from pancreatic adipocytes, which are increased and inflamed in the setting of obesity, though this is typically observed in more advanced stages when tumors invade local fat deposits[14,42]. Moreover, caloric restriction, which blunted tumor progression (**Figure 2f**), only modestly decreases adiposity in *ob/ob* mice[43] and has no significant impact on circulating lipid or glucocorticoid levels (**Supplementary Figure 6a**). Beyond acinar and ductal cells of the exocrine pancreas, the putative origin of PDAC[44,45], the other major cells within the microenvironment reside in the pancreatic islets, which comprise only 1-5% by volume of the pancreas in mice[46]. Therefore, we were surprised to detect significant upregulation of genes associated with pancreatic islet cell function and regeneration (**Figures 3a,b**) in our bulk RNA-Seq analyses. While the expression levels of general neuroendocrine markers typically used to identify islets in pancreatic tissue were unchanged or only mildly elevated in *KCO* pancreata (**Figure 3c**), we saw a marked increase in the expression of genes governing glucose homeostasis and beta islet cell function (**Figure 3d**). We further observed significant upregulation of the *Reg* family of genes (**Figure 3e**), which mediate islet cell regeneration[47]. GLP-1, a proteolytic product of glucagon by prohormone convertase enzymes (*Pcsk1*/*Pcsk2*), is normally detected in the periphery of the murine pancreatic islets, where glucagon-expressing alpha cells reside in non-obese animals[48]. In contrast, in *KCO* mice, we observed expansion of glucagon and GLP-1 production throughout islets including in central areas where insulin-expressing beta cells reside (**Figure 3f**). These observations are consistent with prior research demonstrating increased GLP-1 secretion in islets derived from obese humans and mice[49]. As GLP-1 promotes insulin secretion, these data provide molecular and biochemical evidence for marked islet adaptation within tumors, presumably to maintain glucose homeostasis in the setting of obesity and local tissue injury.

Given that islets may secrete hormones into a portal system intermixed with exocrine cells (the islet-acinar axis)[48,50], we hypothesized that adaptive changes in islet growth factor expression, which promote islet cell expansion and survival in the setting of obesity, could inadvertently play a role in driving exocrine pancreatic tumorigenesis. HFD, *ob/ob*, and *db/db* mice exhibit increased islet size to compensate for peripheral insulin resistance permitting enhanced production and secretion of islet hormones[46]. Indeed, hyperinsulinemia is a prominent feature of obesity, and insulin has been shown to promote proliferation through direct mitogenic action on cancer cells[22]. While we did not observe significant changes in proinsulin gene expression (*Ins1* and *Ins2*) (**Figure 3d**), obesity-associated adaptations included upregulation of endopeptidases that cleave proinsulin to insulin (*Pcsk1* and *Pcsk2*) and factors involved in insulin secretion (*Abcc8* and *Vgf*), which together would be expected to enhance insulin release. Indeed, we confirmed enhanced fasting insulin and C-peptide levels in the serum of *ob/ob* compared to *ob/+* mice (**Supplementary Figure 6b**). To determine whether insulin was directly acting on tumor cells, we evaluated phosphorylation of insulin receptor in PanINs by IHC and found comparable signaling activation in tumors from both non-obese *KC* and obese *KCO* mice (**Supplementary Figure 6c**). These data support a potential role for insulin signaling in pancreatic tumorigenesis, but suggest that additional islet hormones may contribute to cancer development.

In addition to alterations in GLP-1 secretion, prior research has shown that dysregulation of the peptide hormone cholecystokinin (CCK) in islets of obese mice (HFD and *ob/ob*) promotes islet cell survival in the setting of insulin resistance or other stresses[51,52]. CCK is normally synthesized and secreted by enteroendocrine cells of the duodenum to induce pancreatic acinar cell zymogen release for digestion. Yet, we observed that one of the top differentially expressed

genes comparing pancreata from obese *KCO* mice with non-obese *KC* and *KPC* mice was CCK (**Figure 4a; Supplementary Data Table 5)**. Furthermore, IHC confirmed aberrant protein expression of the cleaved active CCK octapeptide (CCK8) predominantly in pancreatic islets cells, including in areas where insulin-expressing beta cells reside (**Figure 4b**). Since exogenous administration of cerulein, a CCK8 analogue, at supraphysiologic levels promotes *Kras*-driven pancreatic tumorigenesis in mice[53], we hypothesized that endogenous islet-derived CCK in the setting of obesity could similarly cooperate locally with oncogenic *Kras* mutation to drive pancreatic cancer development.

If islet-derived CCK were to play a role in early pancreatic tumorigenesis, we reasoned that it must be expressed in the islets of both tumor-bearing and non-tumor-bearing obese mice and that expression must be abolished following weight loss interventions. Indeed, both AAV-Leptin treatment and caloric restriction markedly reduced islet expression of CCK (**Figure 4a; Supplementary Figures 7a,b**). We further confirmed that CCK was expressed in islets from obese (*ob/ob*) mice even in the absence of tumors (**Supplementary Figure 7c**); moreover, pancreatic CCK expression was reduced following AAV-Leptin treatment (**Supplementary Figure 7d**), consistent with islet CCK expression being a general adaptive response to obesity. To determine whether islet CCK expression is evident in human tumors, we performed IHC on pancreata from PDAC patients and observed expression of CCK in ~60% of samples (**Figure 4c**). While CCK expression did not correlate with BMI (**Figure 4d**), cancer-associated weight loss prior to diagnosis may have confounded this analysis. Therefore, we analyzed islets obtained from human donors without known malignancy and observed a positive relationship between BMI and CCK expression (**Figure 4e**). Together, these data demonstrate that obesity promotes

islet CCK expression.

CCK signaling has previously been shown to play a role in pancreatic cancer initiation and maintenance[54]. CCK receptor (CCKR) antagonists impair pancreatic tumor growth in HFD transplant models[55,56] through blockade of the action of dietary fat-induced intestinal CCK on CCKR-expressing tumor cells[57]. Furthermore, the non-selective CCKR antagonist proglumide at doses that block physiologic CCK function impedes tumor progression in non-obese *KC* mice[58]. As circulating CCK levels were not altered in *ob/ob* mice (**Supplementary Figure 7e**), our data implicate obesity-augmented islet CCK expression as a potential driver of early PDAC progression. As a result, we anticipated that proglumide would be insufficient to impair progression in the setting of supraphysiologic local concentrations of CCK in *KCO* mice. Indeed, while proglumide induced the expected systemic pharmacodynamic effect of slowing weight gain[58], no significant impact on tumor development was observed in our model (**Supplementary Figure 5**). To test directly whether islet CCK could contribute to tumor progression, we crossed *MIP-CCK* transgenic mice[52] with *KC* mice to generate non-obese compound transgenic mice (*MKC*: *MIP-CCK; Pdx1-Cre;* $Kras^{LSL\text{-}G12D/WT}$). *MIP-CCK* mice exhibit pancreatic islet-specific CCK expression (**Supplementary Figure 8a**) comparable to *ob/ob* mice without systemic CCK elevation[52]. In support of islet CCK overexpression as a driver of pancreatic ductal tumorigenesis, *MKC* mice exhibited a modest but significant increase in tumor burden compared to *KC* controls, (**Figures 4f,g**). Importantly, the effect of islet CCK on tumor progression did not reach that observed in *KCO* mice, suggesting that additional obesity-associated alterations likely contribute. Nonetheless, these data provide evidence for aberrantly-expressed pancreatic endocrine hormones beyond insulin in driving obesity-associated PDAC.

Finally, we explored the mechanism by which islet-derived CCK promotes tumorigenesis. As exogenous cerulein administration is commonly used as a model for experimental pancreatitis[53], islet CCK could promote tumorigenesis indirectly via its pro-inflammatory effect. Nevertheless, the absence of inflammation or fibrosis in non-tumor-bearing *MIP-CCK* transgenic mice (**Supplementary Figure 8a**) suggests that islet CCK-induced inflammation is not necessary to initiate tumorigenesis. Conversely, acute (cerulein- or arginine-induced) or chronic (cerulein-induced) pancreatitis did not elicit islet CCK expression in mice (**Supplementary Figures 8b,c**). CCK expression was similarly not significantly observed in islets of patients with chronic pancreatitis (**Supplementary Figure 8d**). Based on these data, we conclude that islet CCK may support tumor development independent of inflammation through signaling effects in the microenvironment.

While PDAC is commonly thought to arise from acinar (via acinar-to-ductal metaplasia) or ductal cells[44,45], pancreatic exocrine and endocrine cells express CCK receptors[54]. Indeed, CCK stimulates insulin secretion from beta cells, which in turn could modulate early tumorigenesis. Importantly, *MIP-CCK* mice do not exhibit enhanced beta cell mass or increased insulin secretion (during fasting or following glucose stimulation)[52]. Therefore, the pro-tumorigenic effect of islet CCK likely depends on local signaling to the exocrine pancreas (acinar and/or ductal cells). We propose a model in which obesity fosters early pancreatic tumorigenesis by promoting islet adaptations and endocrine-exocrine CCK signaling which cooperate with oncogenic *Kras* to drive acinar-to-ductal metaplasia (ADM) and PanIN development (**Figure 4h**). Importantly, these islet adaptations, including CCK expression, and tumor progression are

reversed following weight loss, supporting the role of anti-obesity strategies in cancer interception.

In summary, leveraging an autochthonous mouse PDAC model, we have shown that obesity plays a causal and reversible role in early pancreatic tumor formation and progression to advanced disease. While PDAC is generally accepted to originate from exocrine cells[44,45], our data endorse a major role for endocrine cell signaling in tumorigenesis. Furthermore, our studies add to the growing body of evidence that obesity may be pro-tumorigenic through its microenvironmental rather than systemic consequences[37] and provide support for a unifying mechanism linking obesity, changes in the local microenvironment, and tumorigenesis via adaptive islet expression of pro-tumorigenic hormones.

METHODS

Animals studies

Animal studies were approved by the Massachusetts Institute of Technology (MIT) and Yale University Institutional Animal Care and Use Committees (IACUC). All animals were maintained on a mixed background. *ob* (Stock #000632), *db* (Stock #000697), *Pdx1-Cre* (Stock #014647), $p53^{fl/fl}$ (Stock #008462), *MADM11-GT* (Stock #013749), and *MADM11-TG* (Stock #013751) mice were obtained from the Jackson Laboratory. *MIP-CCK* mice[52] were obtained from D. B. Davis of the University of Wisconsin. $LSL\text{-}Kras^{G12D}$, $p53^{R172H/WT}$, $p53^{KO/WT}$, and $Kras^{LA2}$ mice were generated previously by the Jacks lab[23,59-61]. *Pdx1-Cre;* $Kras^{LSL\text{-}G12D/WT}$*(KC), KC; ob/+* and *KC; ob/ob* (*KCO*), *KC; db/+*, *KC; db/db*, $Kras^{LA2}$*; +/+*, and $Kras^{LA2}$*; ob/ob* were

produced by intercrossing mice with the appropriate alleles. *KPC* mice, including *KC; p53*$^{R172H/WT}$; *KC; p53*$^{fl/WT}$, *KC; p53*$^{R172H/fl}$, *KC; p53*$^{fl/fl}$, and *KC; MADM11-GT,p53*^{WT}*/MADM11-TG-p53*^{KO} (*MADM-p53)*, were generated as described previously[31]. Mice were genotyped using tail DNA by the HotShot method. Genotyping primers and protocols have been previously reported[31,52,62]. Animals were monitored at least weekly for signs of morbidity and were euthanized by CO2 asphyxiation when they met euthanasia criteria. Date of euthanasia relative to birth date was used for Kaplan-Meier survival analyses. Weights were monitored using a standard small animal scale. Glucose was measured on a OneTouch Ultra2 glucometer on whole blood collected by tail clip. For serum studies, whole blood was collected from anesthetized mice by retro-orbital bleed or terminal cardiac puncture, allowed to clot for 30 minutes at room temperature, and spun through a serum separator tube (Sarstedt) at 10,000 rpm for 5 min prior to storage at -80°C or analysis. Serum CCK was measured by EIA (RayBiotech, Cat# EIAM-CCK). Serum insulin (RIA, Linco Cat# RI-I3K), C-peptide (ELISA, ALPCO Cat# 80-CPTRT-E01), corticosterone (RIA, MP Biomedicals, LLC), free fatty acids (FFA), and triglycerides (TG) were measured by the Yale Diabetes Research Core.

Mouse treatment studies

For diet studies, *Kras*^{LA2} mice were started on high-fat (60% kcal fat, Research Diets 12492) or low-fat (10% kcal fat, Research Diets 12240J) diet at 4 weeks of age. For drug studies, *KCO* mice were treated with pharmaceutical-grade aspirin (2 mg/mL, Spectrum Chemical Group), metformin (2 mg/mL, Spectrum Chemical Group), and proglumide (0.1 mg/mL, Sigma) in drinking water starting at 6 weeks of age and treated for 6 weeks continuously. Water consumption was measured weekly when treated water was replaced. *KCO* mice drank 7.69 +/-

0.58 (s.d.), 8.95 +/- 2.24, 8.09 +/- 3.21, 9.70 +/- 1.49 mL drinking water daily for untreated (control), aspirin, metformin, and proglumide, respectively. Water intake was not statistically different from control for each treatment condition (two-tailed student's t-test). Based on water consumption, average daily doses were 17.9, 16.2, and 0.97 mg for aspirin, metformin, and proglumide, leading to an average dose exposure of ~456, 436, and 26 mg/kg per day, respectively, in-line with prior studies using these agents[58,63]. Mice were randomized following pre-stratification for gender in all treatment conditions.

Murine tissue preparation, histology, and quantification

Mice were euthanized by CO2 asphyxiation and tissue was dissected, fixed in 10% neutral-buffered formalin overnight, and dehydrated in 70% ethanol prior to paraffin-embedding. Adjacent 5 µm sections were cut and stained with hematoxylin and eosin or picosirius red or subject to immunohistochemistry (IHC). Primary antibodies for IHC are listed below. Mach 2 HRP-labeled anti-mouse, anti-rabbit, or anti-guinea pig micro-polymers (Biocare Medical) were used for primary antibody detection using a Thermo Scientific Autostainer 360. Slides were imaged with a modified Nikon T2R inverted microscope (MVI), 4x/10x/20x/40x objectives, and a 2.8 MP CoolSNAP Dyno CCD camera (Photometrics). Monochromatic red, green, and blue images were merged using ImageJ software (NIH). Percentage of tumor burden was quantified blinded to group on scanned slides (Aperio) by measuring cross-sectional area of tumor-bearing areas (PanIN or PDAC including stroma) relative to measured total pancreas area using ImageJ or QuPath v0.1.2 software.

Antibodies

Antibody Target	Species	Company	Product Number	Application	Dilution
B220	Rat	BD Biosciences	550286	IHC	1:100
Beta-tubulin	Rabbit	Cell Signaling Technology	2128	WB	1:1000
Cd3	Rabbit	Abcam	ab16669	IHC	1:300
Cd45 LCA	Rabbit	Abcam	ab10558	IHC	1:100-1:500
Cdkn2a	Rabbit	Abcam	ab54210	IHC	1:500
Cholecystokinin	Rabbit	Immunostar	20078	IHC	1:4000 (mouse), 1:8000 (human)
Ck19	Rabbit	Abcam	ab133496	IHC	1:800
Erk1/2	Mouse	Cell Signaling Technology	9107	WB	1:1000
F4/80	Rabbit	Invitrogen	ma5-16363	IHC	1:100
Gfp	Rabbit	Cell Signaling Technology	2956	WB	1:1000
Hsp90	Mouse	BD Biosciences	610418	WB	1:10,000
Insulin	Guinea Pig	Accurate Chemical	YNGPSWINS7S	IHC	1:300
Leptin (OB)	Rabbit	Santa Cruz Biotechnology	sc-842	WB	1:200
p53	Rabbit	Novacastra	NCL-p53-CM5p	IHC	1:400
pErk1/2 (T202/Y204)	Rabbit	Cell Signaling Technology	4370	WB	1:1000
pInsR/Igf1R (Y1162/Y1163)	Rabbit	Thermo Scientific	44-804G	IHC	1:100
pStat3 (Y705)	Rabbit	Cell Signaling Technology	9145	WB	1:1000
Smad4	Rabbit	Abcam	ab40759	IHC	1:2000
Stat3	Mouse	Cell Signaling Technology	9139	WB	1:1000
Synaptophysin	Rabbit	Neo Markers	RB-1461	IHC	1:100

WB = western blot, IHC = immunohistochemistry

Adeno-associated virus (AAV) generation

Total RNA was isolated from flash frozen adipose tissue derived from *db/db* mice using Trizol (Ambion) and reverse transcribed with a High Capacity cDNA Reverse Transcription kit (Thermo Fisher Scientific). Murine leptin cDNA was PCR amplified with Primestar high-fidelity PCR mix (Takera) using primers (forward 5'- ATGTGCTGGAGACCCCTGT-3', reverse 5'-TCAGCATTCAGGGCTAACATCCAACT-3') synthesized by the Koch Institute Swanson

Biotechnology Center. Amplified leptin cDNA was cloned into the XhoI and NotI sites of the AAV2 backbone vector (*pFBAAVCAGmcsBgHpa*) provided by the University of Iowa Viral Vector Core (UIVVC), which generated AAV2/1-Leptin using a baculovirus system. AAV2/1-GFP, cloned into the same AAV2 plasmid vector, was purchased from UIVVC. AAV-induced leptin expression was verified in 293T cells by western blotting 48 hours after infection. $1x10^{11}$ AAV viral particles were administered to mice via a single injection in the tibialis anterior muscle and circulating leptin levels were measured in the serum by ELISA (Crystal Chem Cat# 90030).

Murine PDAC cell line derivation, culture, and treatments

Murine *KPC* PDAC (mPDAC) cell lines (7307 and 7310) were isolated from primary autochthonous pancreatic tumors arising in congenic C57/B6 *KC; p53*$^{R172H/WT}$ mice[28]. Briefly, tumors were enzymatically dissociated using a mix of collagenase IV, dispase, and DNAse I (Worthington) at 37°C for 30 minutes with further mechanical dissociation using a gentleMACS dissociator (Miltenyi Biotec). Cell suspensions were passed through a 100 µM filter, washed, and plated in complete media containing DMEM (Corning), 10% FBS (Thermo Fisher Scientific), and penicillin/streptomycin (Sigma). Cells were grown for at least five passages to separate tumor cells from tumor-associated fibroblasts. For signaling studies, cells were grown in serum-free conditions overnight, treated with 100 ng/mL recombinant murine leptin (R&D Systems) in serum-free media, and lysed for protein analysis after 20 min (peak induction of downstream signaling). Viability was assessed 72 hours after treatment with 100 ng/mL leptin using the CellTiter Glo (CTG) assay (Promega).

Generation of leptin receptor knockout mPDAC cells

A single guide RNA (sgRNA) sequence (5'-TGAAAGCCACCAGACCTCGA) targeting exon 8 of the murine leptin receptor (LepR) was ligated into the BsmBI site in *lentiGuide-Puro* (Addgene 52963) with compatible annealed oligos to generate *lentiGuide-Puro-sgLepR*. Lentivirus for *lentiGuide-Puro-sgLepR* and *lentiCas9-blast* (Addgene 52962) were produced by co-transfection of 293T cells with lentiviral backbone, packaging vector (psPAX2), and envelope (VSV-G) using TransIT-LT1 (Mirus Bio). Supernatant was collected at 48 and 72 hours and applied to target cells with 8 μg/mL polybrene (EMD Millipore) for transduction. Transduced 7307 mPDAC cells were treated with 10 μg/mL blasticidin S (Life Technologies) and 2 μg/mL puromycin (Life Technologies) for 7 days. Cells were then sorted into single cells by limiting dilution into 96-well plates to isolate clones. Knockout clones were confirmed by genomic DNA extraction using QuickExtract DNA extraction solution (Epicentre), PCR amplification of the target locus (forward primer: 5'-GGTTCTCAGTGCACGCATTT-3'; reverse primer: 5'-ACAACGATTTTCCTGGCATCT-3') with Q5 polymerase (NEB), and Sanger sequencing of PCR products by the Keck Biotechnology Resource Laboratory at Yale. KO1 clone harbored two frameshift mutant alleles: 32 bp deletion and an 18 bp deletion with a 2 bp insertion (effective 16 bp deletion). KO2 clone also harbored two independent frameshift mutant alleles: 1 bp deletion and a 13 bp deletion.

Immunoblotting

Cells were lysed with ice-cold RIPA buffer (Thermo Fisher Scientific), supplemented with 0.5 μM EDTA and Halt protease and phosphatase inhibitors (Thermo Fisher Scientific), rotated at 4°C for 15-30 minutes to mix, and centrifuged at maximum speed for 15 minutes to collect

whole cell lysates. Protein concentration was measured with the BCA protein assay (Pierce). 30 μg of total protein per sample was loaded into 4-12% NuPAGE Tris-Bis (Thermo Fisher Scientific) or 4-20% Tris-Glycine TGX (Bio-Rad) gradient gels and separated by SDS-PAGE. Proteins were transferred to nitrocellulose (for fluorescence detection) or PVDF (for chemiluminescent detection) membranes and blocked with Odyssey Blocking Buffer (LI-COR) or 5% milk, respectively. Primary antibodies used for immunoblotting are listed above. HSP90 and beta-tubulin were used as loading controls. Primary antibodies were detected with fluorescent DyLight-conjugated (Cell Signaling Technologies) or HRP-conjugated (BioRad) secondary antibodies for fluorescent (LI-COR Odyssey scanner) or chemiluminescent detection (Perkin Elmer ECL), respectively. Quantification of phosphorylated protein levels was performed using Image Studio Lite (LI-COR) and normalized to total protein levels.

DNA and RNA isolation from mouse tumors

Mice were euthanized by cervical dislocation and pancreata were rapidly dissected, flash frozen in liquid nitrogen, and stored at -80C. Prior to DNA and RNA isolation, frozen tumors were mechanically ground in liquid nitrogen using a mortar and pestle. Genomic DNA and total RNA were extracted from ground tumor tissue using a Qiagen Allprep kit per manufacturer's instructions. DNA concentration was measured using Picogreen (Invitrogen). RNA concentration, quality, and purity were determined using an Agilent Bioanalyzer.

Mouse tumor exome sequencing and analysis

Exome capture on mouse tumor genomic DNA was performed by Macrogen using an Agilent Sureselect Mouse All Exon kit. 100-nt paired-end sequencing to a raw sequence depth of 150X

per sample on a HiSeq 2500 (Illumina) was subsequently performed. Variant calls were made using an approach similar to the HaJaVa platform[64]. Reads were processed to remove adapter sequences (using exact matches to 10mer adapter start sequence: AGATCGGAAG) using the FASTX-toolkit (http://hannonlab.cshl.edu/fastx_toolkit). Surviving reads greater than or equal to 15nt in length were retained. Reads were aligned to the mouse mm9 genome assembly (UCSC) using BWA (v0.5.5). Duplicates were removed using Picard (v1.21) MarkDuplicates utility. Local realignment of reads around indels and base quality recalibration were performed using GATK (v1.0.5538). Variant calls were made with GATK UnifiedGenotyper using the mm9 reference sequence in regions targeted by the Agilent capture kit (version G7550_20110119_mm9 from Agilent). Calls with at least 14X read coverage and dual strand support were retained and further filtered using GATK VariantFiltration (arguments -clusterWindowSize 10 -cluster 3), GATK SelectVariants (arguments "SB < -0.1", "QUAL >= 30.0", "QD >= 5.0", "HRun <= 5"), and Sanger Mouse Genomes Project Variant calls[65]. Variants were annotated using Annovar[66] (version 2016Feb01) and mouse dbSNP build 142 (ftp.ncbi.nlm.nih.gov/snp/).

Mouse tumor RNA sequencing (RNA-Seq) and analysis

cDNA libraries from tumor total RNA were prepared by the MIT BioMicro Center using the Neoprep library preparation system (Illumina) with indexed adaptor sequences and polyA selection. Sequencing was performed on an Illumina NextSeq to obtain paired-end 75-nt reads. All reads that passed quality metrics were mapped to UCSC mm9 mouse genome build (http://genome.ucsc.edu/) using RSEM (v1.2.12) (http://deweylab.github.io/RSEM/). All RNA-Seq analyses were conducted in R. High-resolution signature analyses between tumors from

obese (*KCO* and *KCO* treated with AAV-GFP) and non-obese (*KC* and *KPC*) models were performed using a blind source separation methodology based on Independent Component Analysis (ICA), as previously described[7,34]. Gene Set Enrichment Analyses (GSEA) (http://software.broadinstitute.org/gsea/) were carried out using standardized signature correlation scores (for ICA signatures) with default settings. Network representations of GSEA results were generated using EnrichmentMap (http://www.baderlab.org/Software/EnrichmentMap) for Cytoscape v3.3.0 (http://www.cytoscape.org) with $p<0.005$ and FDR<0.1. Each circle represents a gene set with circle size corresponding to gene set size and intensity corresponding to enrichment significance. Red is upregulated and blue is downregulated. Each line corresponds to minimum 50% mutual overlap with line thickness corresponding to degree of overlap. Cellular processes for gene set clusters were manually curated. Tumor suppressor gene mutations in RNA-Seq datasets were called using the GATK Best Practices workflow for SNP calling on RNA-Seq data (software.broadinstitute.org/gatk/documentation/article.php?id=3891). Transcriptomic reads were trimmed to eliminate adapter sequences using an exact 10mer match to the start of the adapter sequence (AGATCGGAAG) using Cutadapt (v1.16) and subsequently mapped to the mouse mm9 (UCSC) genome assembly using the STAR RNA-Seq aligner with default parameters. Picard v2.17.0 MarkDuplicates utility was used to mark duplicates in the aligned data. GATK (v3.8.0) toolkit was used to "SplitNTrim" and reassign mapping qualities as per GATK best practices, and indel realignment and base recalibration were performed as recommended. Variants were called against the mm9 reference sequence using the GATK HaplotypeCaller and filtered using GATK VariantFiltration with recommended parameters. Variant calls were annotated using Annovar (version 2016Feb01). CIBERSORT analysis was

performed using the online tool (http://cibersort.stanford.edu) with the standard LM22 signature file[35]. Genes with standardized signature correlation scores $z > 3$ (alternatively $z < -3$) were used as gene sets to score TCGA (https://tcga-data.nci.nih.gov/tcga/) Pancreatic Adenocarcinoma (PAAD) tumors[5] using ssGSEA[67]. Tumors were stratified based on standardized signature scores (z-scores) derived using ssGSEA. Associated patients within top and bottom buckets (> or < 1 s.d.) were each assessed for over-representation of previously established molecular subtypes (squamous, immunogenic, progenitor, ADEX[4]) using the hypergeometric test.

Evaluation of cancer driver genes in human PDAC biospecimens

Acquisition of resected PDAC biospecimens including institutional review board approval and informed consent procedures were previously described[33]. Pre-operative body-mass index (BMI) and molecular data on the main PDAC driver genes was available for 184 of 356 patients from this prior study. Of note, PDAC patients experience significant weight loss in the months preceding diagnosis, and weight at surgery may therefore not be fully reflective of weight in the prediagnostic period. In 125 patients with available weight data at 6 months before diagnosis, we compared weight at surgery with weight 6 months before diagnosis, and observed a strong correlation (Spearman's rank correlation coefficient = 0.90, $p<0.0001$). This suggests that although weight may decrease in months preceding diagnosis, the rank order of 2 measurements is likely to be highly consistent. Targeted exome sequencing and immunohistochemistry (IHC) have been previously described[33]. We used World Health Organization categories to classify patients as normal weight (<25 kg/m^2), overweight (25-30 kg/m^2), or obese (>30 kg/m^2).

Evaluation of CCK expression in human biospecimens

IHC for detection of CCK8 expression in human PDAC samples was performed on 4 μm sections of formalin-fixed paraffin-embedded tissue blocks containing neoplastic and non-neoplastic pancreatic parenchyma that were obtained as part of specimens resected for pancreatic adenocarcinoma treatment, as previously described[33]. Antigen retrieval was performed using citrate buffer (pH 6.0, Dako) in a 2100 Antigen Retriever system (Electron Microscopy Sciences). Sections were then incubated with dual endogenous peroxidase block (Dako) for 20 minutes at room temperature, protein block (Dako) for 10 minutes at room temperature, and anti-CCK8 primary antibody for 1 hour at 4°C. Chromogenic visualization was subsequently performed using the EnVision+ System- HRP (Dako) with a 3 minute diaminobenzidine (DAB) incubation followed by counterstaining with hematoxylin. For evaluation of CCK8 expression, the surrounding exocrine pancreas served as an internal negative control. If present within the section, neuroendocrine cells within the epithelium of the duodenum served as positive internal controls. The immunohistochemical assessment of CCK8 expression was conducted without knowledge of BMI or other patient data.

Human chronic pancreatitis (etiologies included pancreatic divisum (n=5), Sphincter of Oddi dysfunction (n=2), idiopathic (n=5)) specimens were obtained from 12 adults (ages 25-60, M:F 4:8) undergoing Total Pancreatectomy and Islet Auto-Transplant (TP-IAT) program at the University of Minnesota Medical Center. Pancreatic biopsies were obtained at the time of surgery and processed for routine histologic analyses. Informed consent was obtained from all patients, and the research protocol was reviewed and approved by the University of Minnesota

Institutional Review Board. A total of 127 islets were evaluable, of which 4 harbored rare CCK-positive cells.

108 human islets of northern European descent were isolated at the Oxford Consortium for Islet Transplantation (OXCIT, Oxford, UK) as previously described[68]. All studies were approved by the University of Oxford's "Oxford Tropical Research Ethics Committee" (OxTREC Reference: 2-15), or the Oxfordshire Regional Ethics Committee B (REC reference: 09/H0605/2). All organ donors provided informed consent for use of pancreatic tissue in research. RNA was extracted, sequenced, and analyzed as previously described[69]. Reads per kilobase of CCK transcript per million mapped reads (RPKM) was log2 normalized for analysis. For a subset of donors, BMI was not available, and samples could not be used in analysis. Given limited sample size, low and high BMI groups were specified based on median United States BMI (28.2 kg/m^2) defined by the most recent 2015-2016 National Health and Nutrition Examination Survey (NHANES) (https://www.cdc.gov/nchs/nhanes/index.htm). This also closely approximated median BMI in the donor cohort of 28 kg/m^2

Induction of murine pancreatitis

Acute pancreatitis was induced in adult C57/B6 mice (~25 grams in weight) using cerulein (Sigma, six hourly 50 μg/kg intraperitoneally (IP) injections) or arginine (Sigma, three hourly 3 g/kg IP injections). Mice were euthanized and processed for histology at 12 and/or 48 hours after the first injection. Chronic pancreatitis was induced in adult C57/B6 mice with cerulein given six hourly 50 μg/kg IP injections three times a week for 2 weeks prior to analysis. Acute or chronic PBS-treated mice were used as controls. Two mice from each treatment group were analyzed.

Data, material, and code availability

The datasets generated during and/or analyzed during the current study which contributed to **Figures 3 and 4, Supplementary Figures 3 and 4**, and **Supplementary Data Tables 1-6** are available in the NCBI Sequencing Read Archive (SRA) under accession number PRJNA544740 and the NCBI Gene Expression Omnibus (GEO) under accession number GSE131714. Primary murine PDAC cell lines and constructs are available upon request. Computer code for RNA-Seq signature analysis is available upon request. Other software tools (including version numbers) for exome and RNA-Seq analyses are listed above or referenced.

Statistical analyses

P-values for comparisons of two groups were determined by two-tailed student's t-test (for normally distributed data) or Mann-Whitney test (for non-parametric data) as noted in the figure legends using Prism version 5 (Graphpad). All replicates were included in these analyses and represent measurements from distinct samples (biologic replicates). The log-rank test was used for Kaplan-Meier survival analyses with Prism. Using SAS software (SAS Institute, Inc., Version 9.4), we performed logistic regression adjusted for age at surgery (continuous), gender (men, women), and study site to evaluate the association between BMI (normal, overweight, obese) and driver alterations in human PDAC. We calculated odds ratios (ORs) and 95% confidence intervals (CIs). We used the Kruskal-Wallis test to compare the number of driver alterations across BMI categories. A p-value of <0.05 was used to denote statistical significance. All error bars denote standard error of mean (s.e.m.) unless otherwise denoted.

REFERENCES

1 Rahib, L. *et al.* Projecting cancer incidence and deaths to 2030: the unexpected burden of thyroid, liver, and pancreas cancers in the United States. *Cancer Res* **74**, 2913-2921, doi:10.1158/0008-5472.CAN-14-0155 (2014).

2 Siegel, R. L., Miller, K. D. & Jemal, A. Cancer statistics, 2019. *CA Cancer J Clin* **69**, 7-34, doi:10.3322/caac.21551 (2019).

3 Ryan, D. P., Hong, T. S. & Bardeesy, N. Pancreatic Adenocarcinoma. *New England Journal of Medicine* **371**, 1039-1049, doi:10.1056/NEJMra1404198 (2014).

4 Bailey, P. *et al.* Genomic analyses identify molecular subtypes of pancreatic cancer. *Nature* **531**, 47-52, doi:10.1038/nature16965 (2016).

5 The Cancer Genome Atlas Research Network. Integrated Genomic Characterization of Pancreatic Ductal Adenocarcinoma. *Cancer Cell* **32**, 185-203, doi:10.1016/j.ccell.2017.07.007 (2017).

6 Papke, B. & Der, C. J. Drugging RAS: Know the enemy. *Science* **355**, 1158-1163 (2017).

7 Muzumdar, M. D. *et al.* Survival of pancreatic cancer cells lacking KRAS function. *Nat Commun* **8**, 1090, doi:10.1038/s41467-017-00942-5 (2017).

8 Chen, P. Y. *et al.* Adaptive and Reversible Resistance to Kras Inhibition in Pancreatic Cancer Cells. *Cancer Res* **78**, 985-1002, doi:10.1158/0008-5472.CAN-17-2129 (2018).

9 Larsson, S. C., Orsini, N. & Wolk, A. Body mass index and pancreatic cancer risk: A meta-analysis of prospective studies. *Int J Cancer* **120**, 1993-1998, doi:10.1002/ijc.22535 (2007).

10 Yuan, C. *et al.* Prediagnostic body mass index and pancreatic cancer survival. *J Clin Oncol* **31**, 4229-4234, doi:10.1200/JCO.2013.51.7532 (2013).

11 Zyromski, N. J. *et al.* Obesity potentiates the growth and dissemination of pancreatic cancer. *Surgery* **146**, 258-263, doi:10.1016/j.surg.2009.02.024 (2009).

12 Khasawneh, J. *et al.* Inflammation and mitochondrial fatty acid beta-oxidation link obesity to early tumor promotion. *Proc Natl Acad Sci U S A* **106**, 3354-3359, doi:10.1073/pnas.0802864106 (2009).

13 Philip, B. *et al.* A high-fat diet activates oncogenic Kras and COX2 to induce development of pancreatic ductal adenocarcinoma in mice. *Gastroenterology* **145**, 1449-1458, doi:10.1053/j.gastro.2013.08.018 (2013).

14 Incio, J. *et al.* Obesity-Induced Inflammation and Desmoplasia Promote Pancreatic Cancer Progression and Resistance to Chemotherapy. *Cancer Discovery* **6**, 852-869, doi:10.1158/2159-8290.Cd-15-1177 (2016).

15 Zaytouni, T. *et al.* Critical role for arginase 2 in obesity-associated pancreatic cancer. *Nat Commun* **8**, 242, doi:10.1038/s41467-017-00331-y (2017).

16 Rooman, I. *et al.* Incidence of pancreatic cancer is dramatically increased by a high fat, high calorie diet in KrasG12D mice. *Plos One* **12**, doi:10.1371/journal.pone.0184455 (2017).

17 Speakman, J. R. Use of high-fat diets to study rodent obesity as a model of human obesity. *Int J Obes (Lond)*, doi:10.1038/s41366-019-0363-7 (2019).

18 Olive, K. P. *et al.* Inhibition of Hedgehog signaling enhances delivery of chemotherapy in a mouse model of pancreatic cancer. *Science* **324**, 1457-1461, doi:10.1126/science.1171362 (2009).

19 Massetti, G. M., Dietz, W. H. & Richardson, L. C. Excessive Weight Gain, Obesity, and Cancer: Opportunities for Clinical Intervention. *JAMA* **318**, 1975-1976, doi:10.1001/jama.2017.15519 (2017).

20 Halaas, J. L. *et al.* Weight-reducing effects of the plasma protein encoded by the obese gene. *Science* **269**, 543-546 (1995).
21 Hingorani, S. R. *et al.* Preinvasive and invasive ductal pancreatic cancer and its early detection in the mouse. *Cancer Cell* **4**, 437-450 (2003).
22 Ulrich, C. M., Himbert, C., Holowatyj, A. N. & Hursting, S. D. Energy balance and gastrointestinal cancer: risk, interventions, outcomes and mechanisms. *Nat Rev Gastroenterol Hepatol* **15**, 683-698, doi:10.1038/s41575-018-0053-2 (2018).
23 Johnson, L. *et al.* Somatic activation of the K-ras oncogene causes early onset lung cancer in mice. *Nature* **410**, 1111-1116, doi:10.1038/35074129 (2001).
24 Lauby-Secretan, B. *et al.* Body Fatness and Cancer--Viewpoint of the IARC Working Group. *N Engl J Med* **375**, 794-798, doi:10.1056/NEJMsr1606602 (2016).
25 Xu, M., Jung, X., Hines, O. J., Eibl, G. & Chen, Y. Obesity and Pancreatic Cancer: Overview of Epidemiology and Potential Prevention by Weight Loss. *Pancreas* **47**, 158-162, doi:10.1097/MPA.0000000000000974 (2018).
26 Hendifar, A. E., Chang, J. I., Huang, B. Z., Tuli, R. & Wu, B. U. Cachexia, and not obesity, prior to pancreatic cancer diagnosis worsens survival and is negated by chemotherapy. *J Gastrointest Oncol* **9**, 17-23, doi:10.21037/jgo.2017.11.10 (2018).
27 Usman, M. & Volpi, E. V. DNA damage in obesity: Initiator, promoter and predictor of cancer. *Mutat Res* **778**, 23-37, doi:10.1016/j.mrrev.2018.08.002 (2018).
28 Hingorani, S. R. *et al.* Trp53R172H and KrasG12D cooperate to promote chromosomal instability and widely metastatic pancreatic ductal adenocarcinoma in mice. *Cancer Cell* **7**, 469-483, doi:10.1016/j.ccr.2005.04.023 (2005).
29 Bardeesy, N. *et al.* Smad4 is dispensable for normal pancreas development yet critical in progression and tumor biology of pancreas cancer. *Genes Dev* **20**, 3130-3146, doi:10.1101/gad.1478706 (2006).
30 Bardeesy, N. *et al.* Both p16(Ink4a) and the p19(Arf)-p53 pathway constrain progression of pancreatic adenocarcinoma in the mouse. *Proc Natl Acad Sci U S A* **103**, 5947-5952, doi:10.1073/pnas.0601273103 (2006).
31 Muzumdar, M. D. *et al.* Clonal dynamics following p53 loss of heterozygosity in Kras-driven cancers. *Nat Commun* **7**, 12685, doi:10.1038/ncomms12685 (2016).
32 Bailey, M. H. *et al.* Comprehensive Characterization of Cancer Driver Genes and Mutations. *Cell* **173**, 371-385 e318, doi:10.1016/j.cell.2018.02.060 (2018).
33 Qian, Z. R. *et al.* Association of Alterations in Main Driver Genes With Outcomes of Patients With Resected Pancreatic Ductal Adenocarcinoma. *JAMA Oncol* **4**, e173420, doi:10.1001/jamaoncol.2017.3420 (2018).
34 Hyvarinen, A. & Oja, E. Independent component analysis: algorithms and applications. *Neural Netw* **13**, 411-430 (2000).
35 Newman, A. M. *et al.* Robust enumeration of cell subsets from tissue expression profiles. *Nat Methods* **12**, 453-457, doi:10.1038/nmeth.3337 (2015).
36 Clark, C. E. *et al.* Dynamics of the immune reaction to pancreatic cancer from inception to invasion. *Cancer Res* **67**, 9518-9527, doi:10.1158/0008-5472.CAN-07-0175 (2007).
37 Olson, O. C., Quail, D. F. & Joyce, J. A. Obesity and the tumor microenvironment. *Science* **358**, 1130-1131, doi:10.1126/science.aao5801 (2017).
38 Zhang, Y. P., Wan, Y. D., Sun, Y. L., Li, J. & Zhu, R. T. Aspirin might reduce the incidence of pancreatic cancer: A meta-analysis of observational studies. *Sci Rep* **5**, 15460, doi:10.1038/srep15460 (2015).

39 Li, D., Yeung, S. C., Hassan, M. M., Konopleva, M. & Abbruzzese, J. L. Antidiabetic therapies affect risk of pancreatic cancer. *Gastroenterology* **137**, 482-488, doi:10.1053/j.gastro.2009.04.013 (2009).
40 Rangarajan, S. *et al.* Metformin reverses established lung fibrosis in a bleomycin model. *Nat Med* **24**, 1121-1127, doi:10.1038/s41591-018-0087-6 (2018).
41 Chen, K. *et al.* Metformin suppresses cancer initiation and progression in genetic mouse models of pancreatic cancer. *Mol Cancer* **16**, 131, doi:10.1186/s12943-017-0701-0 (2017).
42 Gomez-Chou, S. B. *et al.* Lipocalin-2 Promotes Pancreatic Ductal Adenocarcinoma by Regulating Inflammation in the Tumor Microenvironment. *Cancer Res* **77**, 2647-2660, doi:10.1158/0008-5472.CAN-16-1986 (2017).
43 van den Hoek, A. M. *et al.* Leptin deficiency per se dictates body composition and insulin action in ob/ob mice. *J Neuroendocrinol* **20**, 120-127, doi:10.1111/j.1365-2826.2007.01626.x (2008).
44 Ray, K. C. *et al.* Epithelial tissues have varying degrees of susceptibility to Kras(G12D)-initiated tumorigenesis in a mouse model. *PLoS One* **6**, e16786, doi:10.1371/journal.pone.0016786 (2011).
45 Kopp, J. L. *et al.* Identification of Sox9-dependent acinar-to-ductal reprogramming as the principal mechanism for initiation of pancreatic ductal adenocarcinoma. *Cancer Cell* **22**, 737-750, doi:10.1016/j.ccr.2012.10.025 (2012).
46 Bock, T., Pakkenberg, B. & Buschard, K. Increased islet volume but unchanged islet number in ob/ob mice. *Diabetes* **52**, 1716-1722 (2003).
47 Li, Q. *et al.* Reg2 Expression Is Required for Pancreatic Islet Compensation in Response to Aging and High-Fat Diet-Induced Obesity. *Endocrinology* **158**, 1634-1644, doi:10.1210/en.2016-1551 (2017).
48 Barreto, S. G., Carati, C. J., Toouli, J. & Saccone, G. T. The islet-acinar axis of the pancreas: more than just insulin. *Am J Physiol Gastrointest Liver Physiol* **299**, G10-22, doi:10.1152/ajpgi.00077.2010 (2010).
49 Linnemann, A. K. *et al.* Glucagon-Like Peptide-1 Regulates Cholecystokinin Production in beta-Cells to Protect From Apoptosis. *Mol Endocrinol* **29**, 978-987, doi:10.1210/me.2015-1030 (2015).
50 Williams, J. A. & Goldfine, I. D. The insulin-pancreatic acinar axis. *Diabetes* **34**, 980-986 (1985).
51 Lavine, J. A. *et al.* Cholecystokinin is up-regulated in obese mouse islets and expands beta-cell mass by increasing beta-cell survival. *Endocrinology* **151**, 3577-3588, doi:10.1210/en.2010-0233 (2010).
52 Lavine, J. A. *et al.* Cholecystokinin expression in the beta-cell leads to increased beta-cell area in aged mice and protects from streptozotocin-induced diabetes and apoptosis. *Am J Physiol Endocrinol Metab* **309**, E819-828, doi:10.1152/ajpendo.00159.2015 (2015).
53 Guerra, C. *et al.* Chronic pancreatitis is essential for induction of pancreatic ductal adenocarcinoma by K-Ras oncogenes in adult mice. *Cancer Cell* **11**, 291-302, doi:10.1016/j.ccr.2007.01.012 (2007).
54 Smith, J. P. & Solomon, T. E. Cholecystokinin and pancreatic cancer: the chicken or the egg? *Am J Physiol Gastrointest Liver Physiol* **306**, G91-G101, doi:10.1152/ajpgi.00301.2013 (2014).

55 Matters, G. L. *et al.* Cholecystokinin mediates progression and metastasis of pancreatic cancer associated with dietary fat. *Dig Dis Sci* **59**, 1180-1191, doi:10.1007/s10620-014-3201-8 (2014).
56 Smith, J. P., Wang, S., Nadella, S., Jablonski, S. A. & Weiner, L. M. Cholecystokinin receptor antagonist alters pancreatic cancer microenvironment and increases efficacy of immune checkpoint antibody therapy in mice. *Cancer Immunol Immunother* **67**, 195-207, doi:10.1007/s00262-017-2077-9 (2018).
57 Nadella, S. *et al.* Dietary fat stimulates pancreatic cancer growth and promotes fibrosis of the tumor microenvironment through the cholecystokinin receptor. *Am J Physiol Gastrointest Liver Physiol* **315**, G699-G712, doi:10.1152/ajpgi.00123.2018 (2018).
58 Smith, J. P. *et al.* Cholecystokinin Receptor Antagonist Halts Progression of Pancreatic Cancer Precursor Lesions and Fibrosis in Mice. *Pancreas* **43**, 1050-1059, doi:10.1097/mpa.0000000000000194 (2014).
59 Jackson, E. L. *et al.* Analysis of lung tumor initiation and progression using conditional expression of oncogenic K-ras. *Genes Dev* **15**, 3243-3248, doi:10.1101/gad.943001 (2001).
60 Olive, K. P. *et al.* Mutant p53 gain of function in two mouse models of Li-Fraumeni syndrome. *Cell* **119**, 847-860, doi:10.1016/j.cell.2004.11.004 (2004).
61 Jacks, T. *et al.* Tumor spectrum analysis in p53-mutant mice. *Curr Biol* **4**, 1-7 (1994).
62 Ellett, J. D., Evans, Z. P., Zhang, G., Chavin, K. D. & Spyropoulos, D. D. A rapid PCR-based method for the identification of ob mutant mice. *Obesity (Silver Spring)* **17**, 402-404, doi:10.1038/oby.2008.443 (2009).
63 Chandel, N. S. *et al.* Are Metformin Doses Used in Murine Cancer Models Clinically Relevant? *Cell Metab* **23**, 569-570, doi:10.1016/j.cmet.2016.03.010 (2016).
64 McFadden, D. G. *et al.* Mutational landscape of EGFR-, MYC-, and Kras-driven genetically engineered mouse models of lung adenocarcinoma. *Proc Natl Acad Sci U S A* **113**, E6409-E6417, doi:10.1073/pnas.1613601113 (2016).
65 Keane, T. M. *et al.* Mouse genomic variation and its effect on phenotypes and gene regulation. *Nature* **477**, 289-294, doi:10.1038/nature10413 (2011).
66 Wang, K., Li, M. & Hakonarson, H. ANNOVAR: functional annotation of genetic variants from high-throughput sequencing data. *Nucleic Acids Res* **38**, e164, doi:10.1093/nar/gkq603 (2010).
67 Barbie, D. A. *et al.* Systematic RNA interference reveals that oncogenic KRAS-driven cancers require TBK1. *Nature* **462**, 108-112, doi:10.1038/nature08460 (2009).
68 Cross, S. E., Hughes, S. J., Clark, A., Gray, D. W. & Johnson, P. R. Collagenase does not persist in human islets following isolation. *Cell Transplant* **21**, 2531-2535, doi:10.3727/096368912X636975 (2012).
69 van de Bunt, M. *et al.* Transcript Expression Data from Human Islets Links Regulatory Signals from Genome-Wide Association Studies for Type 2 Diabetes and Glycemic Traits to Their Downstream Effectors. *PLoS Genet* **11**, e1005694, doi:10.1371/journal.pgen.1005694 (2015).

ACKNOWLEDGEMENTS

We thank F. Gorelick and F. Wilson for critical reading of the manuscript; R. Kibbey and R. Perry for helpful discussions; K. Mercer and C. Garcia for technical assistance; K. Cormier and C. Condon from the Hope Babette Tang (1983) Histology Facility and A. Brooks, P. Gaule, Y. Bai, B. Acs, and D. Rhim from Yale Pathology Tissue Services for histology assistance; M. Robert and R. Bronson for pathology assistance; S. Levine, V. Dayal, and J. Penterman from the MIT BioMicro Center for RNA-Seq support; the University of Iowa Viral Vector core for AAV constructs and generation; M. Batsu and R. Jacobs from the Yale Diabetes Research Core for serum ELISA/RIA studies; the Oxford Human Islet Isolation facility for the provision of human islets for research; T. Kolodecik and F. Gorelick for providing murine pancreatitis specimens; F. Zheng for CRISPR constructs; and A. Berns, D. B. Davis, A. Lowy, L. Luo, and Jackson Laboratories for mice. This work was supported in part by a Lustgarten Foundation Research Investigator Grant (C.S.F. and M.D.M.), Cancer Center Support (core) grants P30-CA016359 (C.S.F.) and P30-CA014051 (T.J.) from the National Cancer Institute, a Pilot Grant from the Yale Cancer Center (M.D.M.), and a Yale Cancer Innovations Award (M.D.M.). The National Institute for Health Research, Oxford Biomedical Research Centre funded islet provision at the Oxford Human Islet Isolation facility. A.B. is funded by an NCI Mentored Cancer Prevention, Control, Behavioral Sciences, and Population Sciences Career Development Award (K07CA222159) and a Bob Parsons Fellowship. A.L.G. is a Wellcome Senior Fellow in Basic Biomedical Science. Her work was funded in Oxford by the Wellcome Trust (095101, 200837, 106130, 203141, Medical Research Council (MR/L020149/1), European Union Horizon 2020 Programme (T2D Systems), and NIH (U01-DK105535; U01-DK085545*)*. M.I.M. is a Wellcome Senior Investigator and an NIHR Senior Investigator. Relevant funding support for this work

comes from Wellcome (090532, 106130, 098381, 203141, 212259), NIDDK (U01-DK105535), and NIHR (NF-SI-0617-10090). The views expressed in this article are those of the author(s) and not necessarily those of the NHS, the NIHR, or the Department of Health. B.M.W. acknowledges support from the Hale Family Center for Pancreatic Cancer Research, Lustgarten Foundation, NIH U01-CA210171, Stand Up to Cancer, Noble Effort Fund, Wexler Family Fund, and Promises for Purple. T.J. is a Howard Hughes Medical Institute Investigator, the David H. Koch Professor of Biology, and a Daniel K. Ludwig Scholar. M.D.M. is supported by an NCI Mentored Clinical Scientist Research Career Development Award (K08CA2080016) and was supported by a KL2/Catalyst Medical Research Investigator Training award (an appointed KL2 award) from Harvard Catalyst | The Harvard Clinical and Translational Science Center (National Center for Research Resources and the National Center for Advancing Translational Sciences) (KL2 TR001100), a Conquer Cancer Foundation-American Society for Clinical Oncology (CCF-ASCO) Young Investigator Award, a Career Development Award from the Dana-Farber Cancer Institute/Harvard Cancer Center SPORE in Gastrointestinal Cancer, and the NIH Loan Repayment Program. The content is solely the responsibility of the authors and does not necessarily represent the official views of the National Institutes of Health.

AUTHOR CONTRIBUTIONS

T.J., C.S.F., and M.D.M. designed and supervised the study; K.M.C., J.S., L.L., K.J.D., R.R., and M.D.M. performed experiments; A.B. conducted bioinformatics analyses on murine exome and RNA-Seq data; A.B., J.N., S.A.V., A.D.C., and B.M.W. performed targeted exome and IHC analyses on human PDAC biospecimens; D.T.C., R.F.D., A.F.H., and A.C.K. provided human PDAC biospecimens for analysis; J.J.W. and M.D.B. provided human chronic pancreatitis

biospecimens; V.N., A.L.G., and M.I.M. acquired and analyzed human donor islet gene expression data; M.D.M. wrote the manuscript with comments from all authors.

COMPETING FINANCIAL INTERESTS

M.D.B. acknowledges research support from ViaCyte and Dexcom and serves on the medical advisory boards for Novo Nordisk and ARIEL Precision Medicine. A.L.G. has received honoraria from Merck and Novo Nordisk and has received research funding from Novo Nordisk. M.I.M. serves on advisory panels for Pfizer, Novo Nordisk, Zoe Global; has received honoraria from Merck, Pfizer, Novo Nordisk and Eli Lilly; has stock options in Zoe Global; has received research funding from Abbvie, Astra Zeneca, Boehringer Ingelheim, Eli Lilly, Janssen, Merck, Novo Nordisk, Pfizer, Roche, Sanofi Aventis, Servier & Takeda. B.M.W. declares research funding from Celgene Inc. and Eli Lilly & Company, and consulting for BioLineRx Ltd., Celgene Inc., G1 Therapeutics Inc., and GRAIL Inc. T.J. is a Board of Directors member and equity holder of Amgen and Thermo Fisher Scientific; co-Founder and Scientific Advisory Board member of Dragonfly Therapeutics, co-founder of T2 Biosystems, and Scientific Advisory Board member of SQZ Biotech with equity holding in all three companies; he receives funding from the Johnson & Johnson Lung Cancer Initiative and Calico. C.S.F. reports receiving personal fees from Eli Lilly, Entrinsic Health, Pfizer, Merck, Sanofi, Roche, Genentech, Merrimack Pharma, Dicerna, Bayer, Celgene, Agios, Gilead Sciences, Five Prime Therapeutics, Taiho, KEW, and CytomX Therapeutics and receiving support from CytomX Therapeutics.

CORRESPONDENCE

Correspondence and requests for materials should be addressed to mandar.muzumdar@yale.edu.

MAIN FIGURES

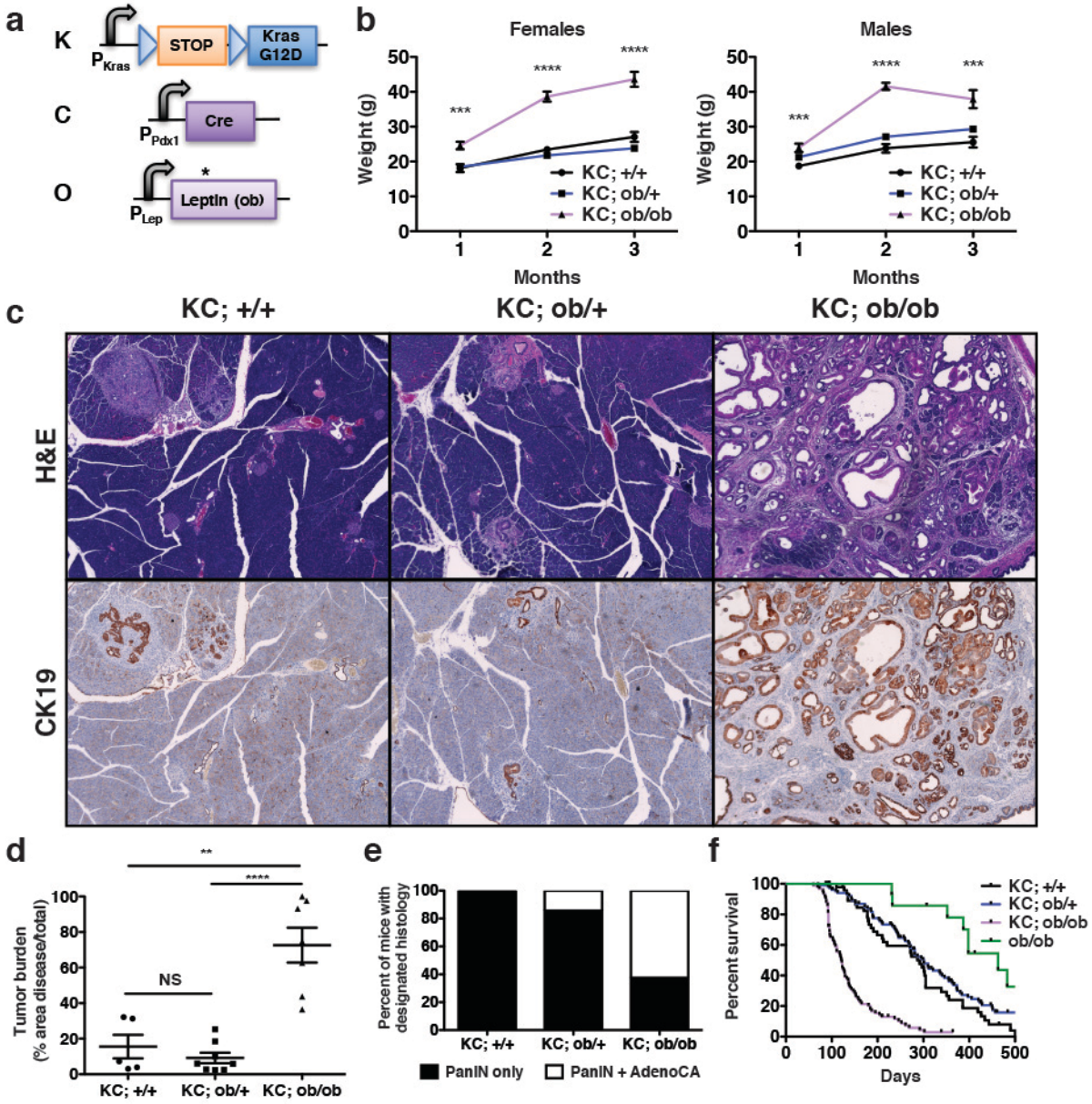

Figure 1. Accelerated PDAC progression in *KCO* mice.

a) Schematic of transgenic/knock-in alleles in leptin-deficient *KC* mice (*KC; ob/ob* or *KCO*). Black arrows denote promoters. *Kras* and *Lep* promoters are endogenous. Blue triangles denote LoxP sites. A STOP cassette prevents oncogenic *Kras* (*G12D*) expression prior to Cre-mediated recombination. * denotes point mutation in *ob* gene causing premature stop.

b) Average body weight +/- s.e.m. (in grams) of male and female *KC* mice of varying *ob* genotype over time (n=22-46 mice per group). ***p<0.001, ****p<0.0001 compared to *KC; +/+* mice, two-tailed student's t-test at each time point.

c) Representative histologic sections of pancreata from mice of designated genotypes at 3 months of age demonstrated differences in the generation of CK19-positive ductal tumors. Scale bar: 200 μm.

d) Tumor burden (average % cross-sectional area of disease/total +/- s.e.m.) in mice of designated genotypes at 3 months of age (n=5-8 mice per group). **p<0.01, ****p<0.0001, two-tailed student's t-test. NS = non-significant.

e) Percentage of mice of particular genotypes harboring PanINs and/or adenocarcinoma by histology at 3 months of age (n=5-8 mice/group).

f) Kaplan-Meier survival curves for non-obese *KC* mice (*KC; +/+* (n=51), non-obese *KC; ob/+* (n=106)), obese *KC* mice (*KC; ob/ob*, *KCO*, n=91), and obese non-tumor bearing controls (*ob/ob* (n=14)). Log-rank test: p<0.0001 *KC; +/+* vs. *KC; ob/ob*, p<0.0001 *KC; ob/+* vs. *KC; ob/ob*, p>0.05 *KC; +/+* vs. *KC; ob/+*.

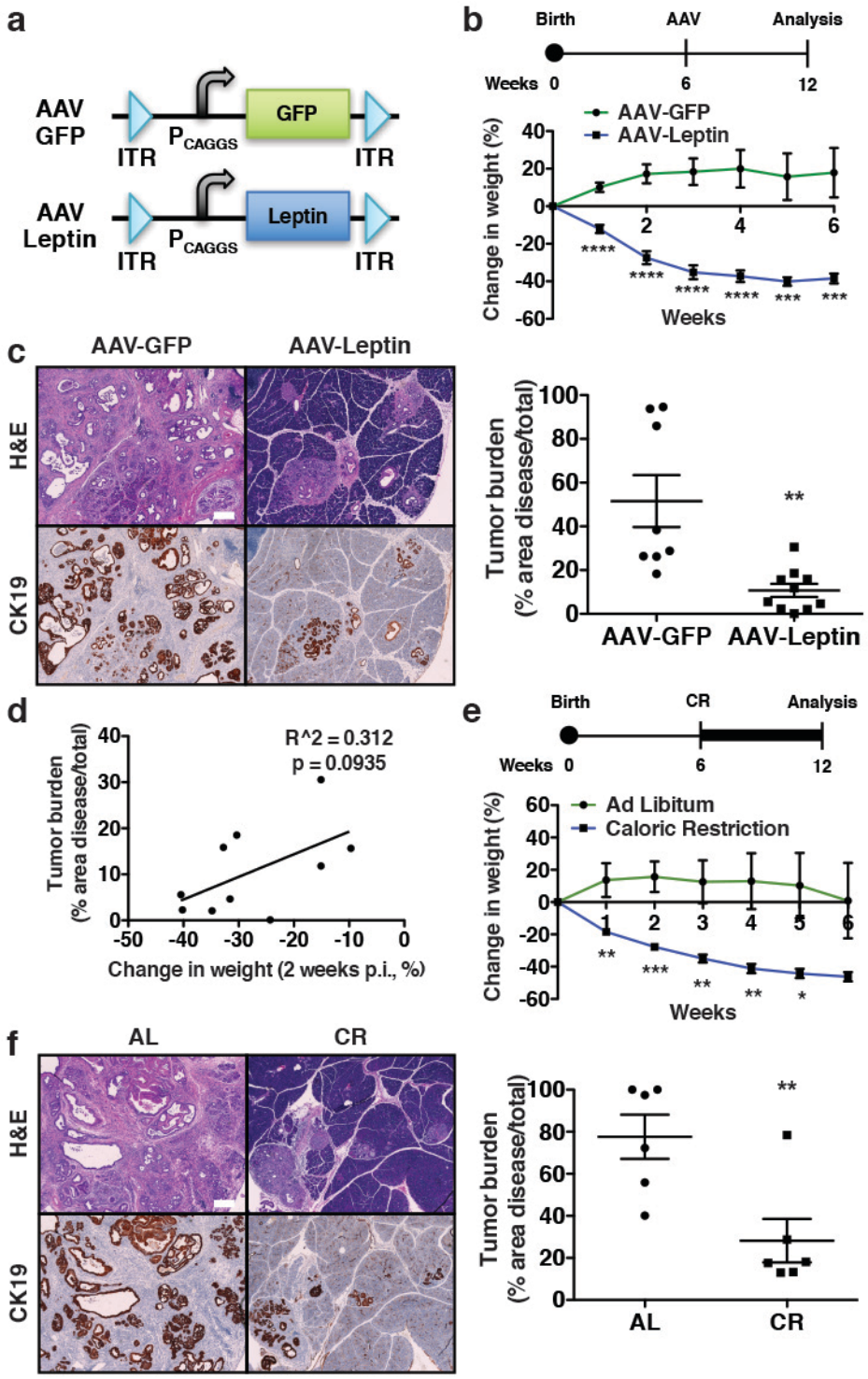

Figure 2. Weight loss intercepts tumor progression in *KCO* mice.

a) Schematic of AAV vectors administered to *KCO* mice. ITR = internal tandem repeat for AAV2. CAGGS = CMV enhancer chicken beta-actin promoter. Leptin is murine cDNA.

GFP is control.

b) Schematic of AAV treatment for tumor interception experiment. AAV was administered at 6 weeks of age prior to development of significant tumor burden. Mice were analyzed 6 weeks later. Average percent change in body weight +/- s.e.m (n=8-10 mice/group) following AAV administration is shown.

c) Representative histologic sections of pancreata of mice at endpoint demonstrate a reduction in CK19-positive ductal tumors with AAV-Leptin. Quantification of tumor burden (average % cross-sectional area of disease/total +/- s.e.m.) is shown (n=8-10 mice/group).

d) Percent change in body weight (2 weeks post infection (p.i.)) from (C) plotted against tumor burden in (E) of AAV-Leptin-infected *KCO* mice. Each point represents one mouse (n=10). Greater weight loss is associated with less tumor burden. R^2 and p-values are shown for linear regression

e) Schematic for caloric restriction (CR) experiment. Mice began caloric restriction (1g/mouse/day of food) at 6 weeks of age as in (B). Controls remained on ad libitum diet (AL). Average percent change in body weight +/- s.e.m (n=6 mice/group) following intervention is shown.

f) Representative histologic sections of pancreata of mice at endpoint demonstrate a reduction in CK19-positive ductal tumors with caloric restriction. Quantification of tumor burden (average % cross-sectional area of disease/total +/- s.e.m.) is shown (n=6 mice/group).

* $p<0.05$, ** $p<0.01$, *** $p<0.001$, **** $p<0.0001$, two-tailed student's t-test for all pairwise comparisons. Scale bars: 200 μm.

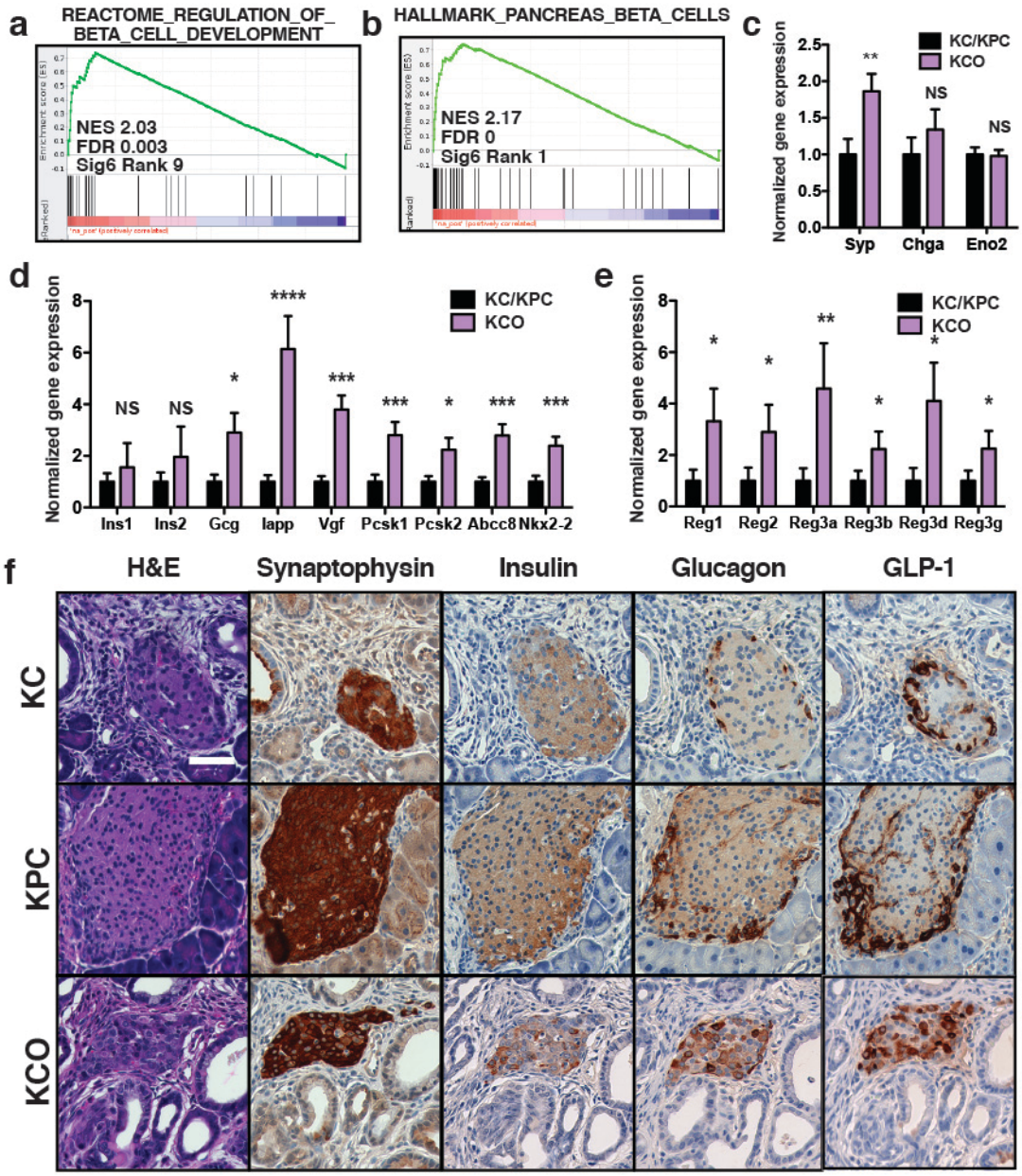

Figure 3. Pancreatic islet adaptation in *KCO* tumors.

a) Gene set enrichment analysis (GSEA) using the curated gene set collection (C2 in MSigDB) revealed an association between *KCO* tumors and genes expressed in beta islet cell development. Normalized enrichment score (NES), false discovery rate (FDR), MSigDB gene set rank (for C2 sets), and the ICA signature (*KCO* vs. *KC*/*KPC*) used in the analysis are shown.

b) GSEA showed an association between *KCO* tumors and genes expressed in beta islet cells based on comparison to the hallmark genes set collection (H in MSigDB).

c) Normalized gene expression (mean RNA-Seq expression counts +/- s.e.m. normalized to non-obese *KC/KPC* tumors) for general neuroendocrine markers observed in pancreatic islet cells (synaptophysin (*Syp*), chromogranin A (*Chga*), and neuron-specific enolase (*Eno2*)), showed mild to no significant difference between *KCO* (n=15) and *KC/KPC* (n=17) mice.

d) Normalized expression (mean RNA-Seq expression counts +/- s.e.m. normalized to non-obese models) of genes involved in glucose homeostasis in pancreatic islet cells revealed marked upregulation in *KCO* mice compared to non-obese models. Neuropeptide precursor hormones (glucagon (*Gcg*), islet amyloid polypeptide (*Iapp*), *Vgf*), endopeptidases (*Pcsk1*, *Pcsk2*), the sulfonyl receptor (*Abcc8*), and beta cell transcription factors (*Nkx2-2*) were upregulated.

e) Normalized expression (mean RNA-Seq expression counts +/- s.e.m. normalized to non-obese models) of genes involved in pancreatic islet cell regeneration.

f) Immunohistochemistry showed aberrant glucagon and GLP-1 expression throughout pancreatic islets in *KCO* mice compared to non-obese controls, consistent with upregulation of Gcg and Pcsk1/Pcsk2 observed by RNA-Seq in (d). Scale bar: 50 μm.

* $p<0.05$, ** $p<0.01$, *** $p<0.001$, **** $p<0.0001$, two-tailed Mann-Whitney test, comparing *KCO to KC/KPC* expression for each gene.

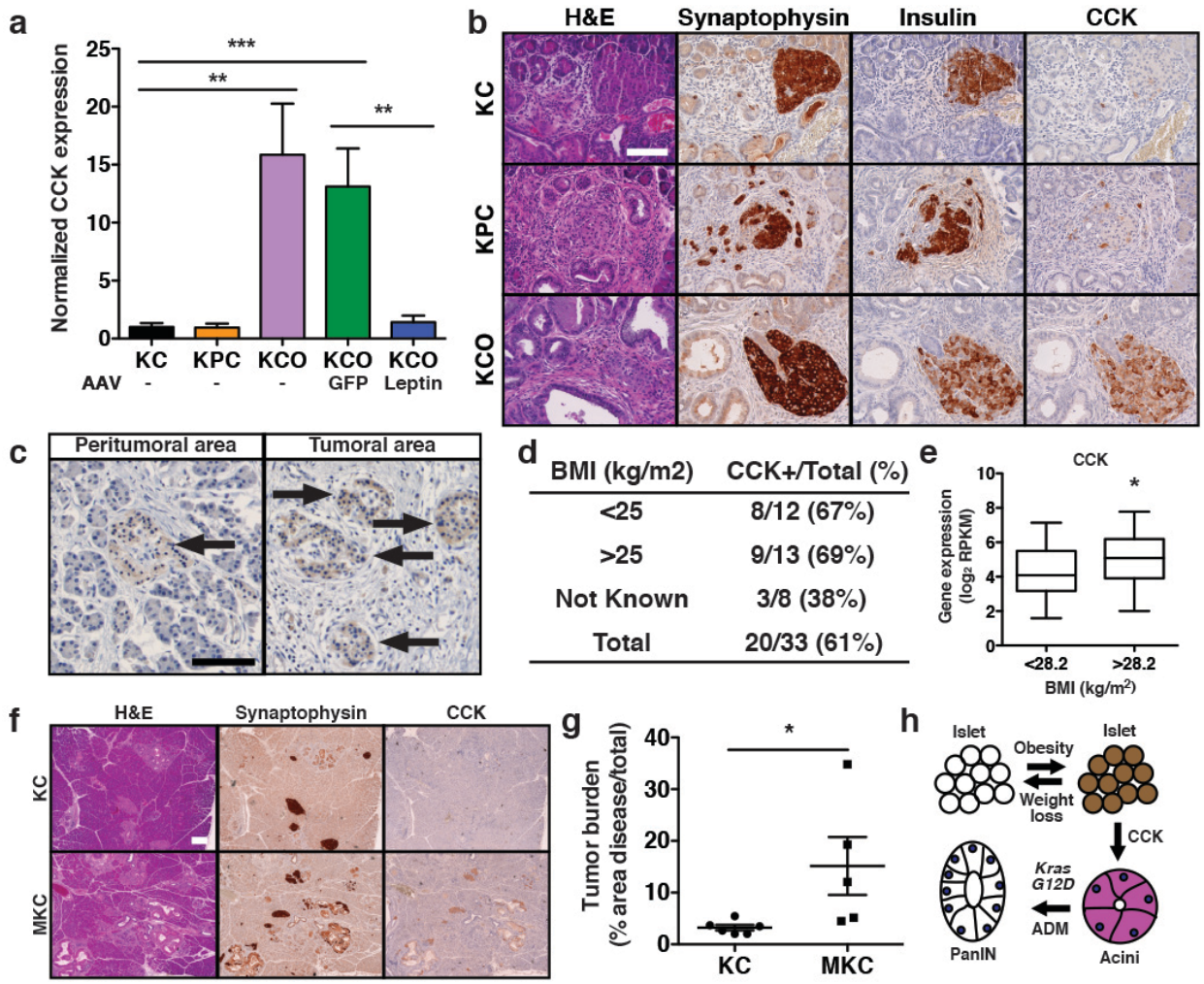

Figure 4. Islet-derived cholecystokinin promotes pancreatic ductal cancer development

a) Normalized expression (mean RNA-Seq expression counts +/- s.e.m. normalized to *KC* tumors) of cholecystokinin (CCK) in obese (*KCO* and *KCO* mice treated with AAV-GFP) and non-obese models (*KC*, *KPC*, and *KCO* mice treated with AAV-Leptin) (n=5-9 per group). **p<0.01, ***p<0.001, two-tailed Mann-Whitney test.

b) CCK was aberrantly overexpressed in pancreatic islets (synaptophysin-positive) of *KCO* compared to *KC* and *KPC* mice, including in insulin-producing cells. Scale bar: 100 µm.

c) CCK was expressed specifically in islet cells (arrows) in human PDAC by immunohistochemistry (IHC) in intra-tumoral and peri-tumoral areas. Scale bar: 100 µm.

d) The majority of human PDAC specimens displayed islet expression by IHC at all BMI levels (<25 kg/m^2 (normal) and >25 kg/m^2 (overweight or obese)).

e) CCK expression in isolated pancreatic islets from human donors with high BMI (n=53, above median US BMI of 28.2 kg/m^2) was significantly (*$p<0.05$, two-tailed Mann-Whitney test) greater than those from low BMI donors (n=55, below median). Box and whisker plots (boxes denote 25th-75th percentile, error bars denote min/max) are shown.

f) Representative histologic sections of pancreata demonstrate an increase in tumorigenesis in *MKC* mice compared to *KC* mice. *MKC* mice exhibit islet-specific (synaptophysin-positive) expression of CCK by IHC. Scale bar: 200 μm.

g) Quantification of tumor burden (average % cross-sectional area of disease/total +/- s.e.m.) in *KC* and *MKC* mice at 3 months (n=5-6 mice/group). * $p<0.05$, two-tailed student's t-test.

h) Model for obesity-associated islet adaptations in PDAC development. Brown denotes CCK expression. ADM = acinar-to-ductal metaplasia.

SUPPLEMENTARY FIGURES AND TABLES

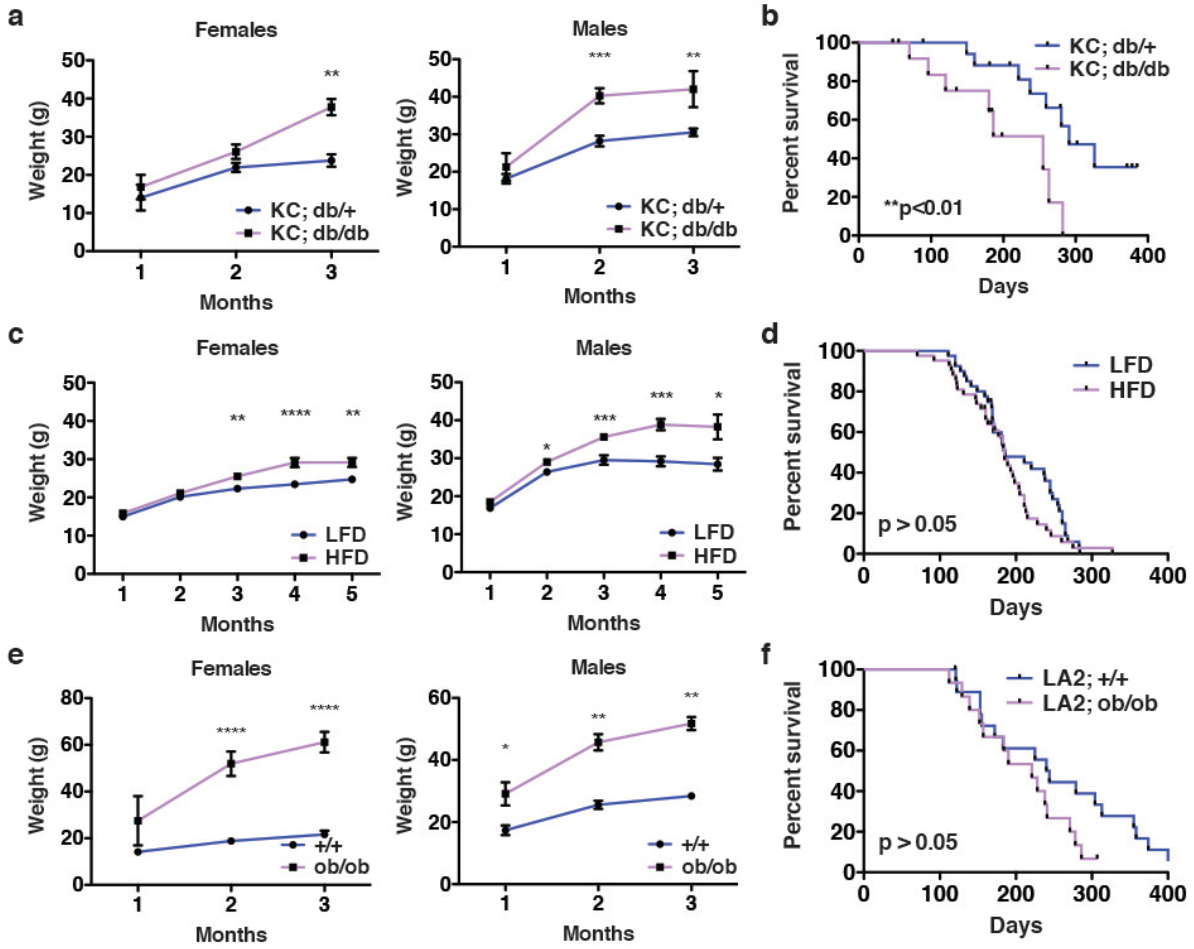

Supplementary Figure 1. Obesity drives pancreatic but not lung tumorigenesis in mice.

a) Average body weight +/- s.e.m. (in grams) of female and male *KC* mice of varying *db* genotype over time (n=4-12 mice per group).

b) Kaplan-Meier survival curves for non-obese (*db/+*, n=18) and obese (*db/db*, n=14) *KC* mice.

c) Average body weight +/- s.e.m. (in grams) of female and male $Kras^{LA2}$ mice fed low-fat (LFD) or high-fat (HFD) diet (n=18-20 mice per group).

d) Kaplan-Meier survival curves for LFD- (n=40) and HFD-fed (n=42) $Kras^{LA2}$ mice.

e) Average body weight +/- s.e.m. (in grams) of female and male *Kras*^{LA2} mice of varying *ob* genotype (n=3-9 mice per group).

f) Kaplan-Meier survival curves for non-obese (+/+, n=19) and obese (*ob/ob*, n=15) *Kras*^{LA2} mice.

*p<0.05, **p<0.01, ***p<0.001, ****p<0.0001, two-tailed student's t-test for all pairwise comparisons.

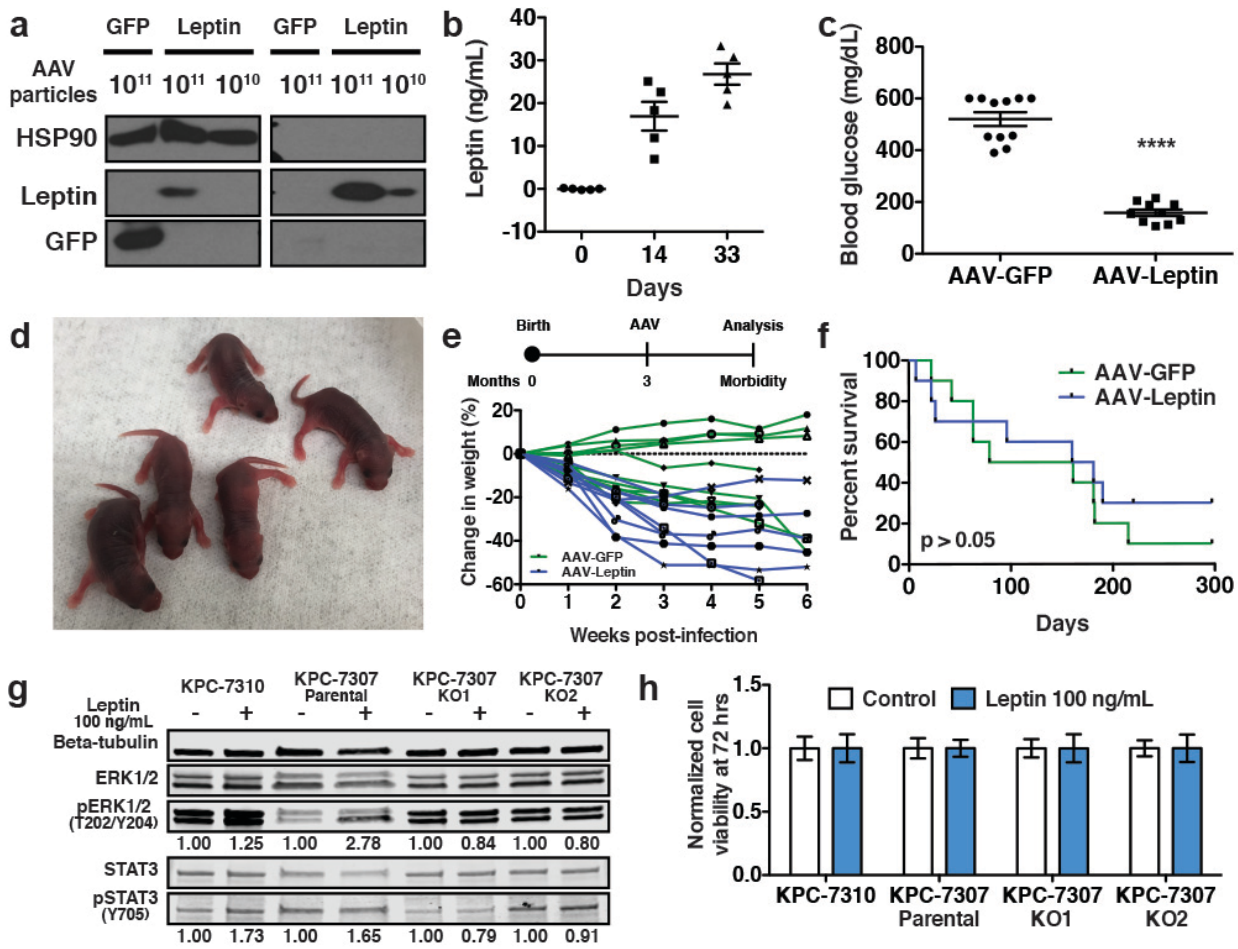

Supplementary Figure 2. Adeno-associated virus-induced leptin expression in cells and mice.

a) Western blot showed dose-dependent leptin protein expression and secretion in 293T cells 48 hours after infection with AAV-Leptin or AAV-GFP control. HSP90 is cellular loading control.

b) ELISA measurement of serum leptin concentrations (mean +/- s.e.m) at 0, 14, and 33 days following intramuscular injection of AAV-Leptin in adult *ob/ob* mice shows sustained expression. X-axis is time (in days) post-infection with AAV.

c) AAV-Leptin induced a reduction in random blood glucose (mean +/- s.e.m.) 6 weeks post-infection of *KCO* mice. **** $p<0.0001$, two-tailed student's t-test. Mice were infected at 6 weeks of age.

d) AAV-Leptin restored fertility in *ob/ob* male and female mice. Shown are early postnatal progeny born from an AAV-Leptin-treated *ob/ob* female mated with an AAV-Leptin-treated *ob/ob* male.

e) Schematic of AAV treatment of tumor-bearing mice. AAV is administered at 3 months of age once tumors have progressed. Percent change in body weight for each mouse (n=10 mice/group) following AAV administration is shown.

f) Kaplan-Meier survival curves for mice in (E) shows no significant difference ($p>0.05$, log-rank test) between AAV treatments (n=10 mice/group).

g) Recombinant murine leptin (100 ng/mL) induces MAPK (pERK1/2) and STAT3 (pSTAT3) signaling in murine *Kras*/*p53* mutant PDAC (mPDAC) cells (KPC-7307 and KPC-7310), which is abolished in leptin receptor knockout clones (KPC-7307 KO1 and KO2). Western blot shows protein levels at 20 minutes following treatment (peak induction). Quantification of pERK/ERK and pSTAT3/STAT3 levels (normalized to untreated) is shown. Beta-tubulin is additional loading control. Leptin dose was chosen to be within an order of magnitude of that observed in the serum of AAV-Leptin-treated mice in (b).

h) Recombinant murine leptin (100 ng/mL) has no effect ($p>0.05$, two-tailed student's t-test) on mPDAC cell viability (+/- s.d., normalized to untreated) 72 hours are treatment (n=5 replicates/condition).

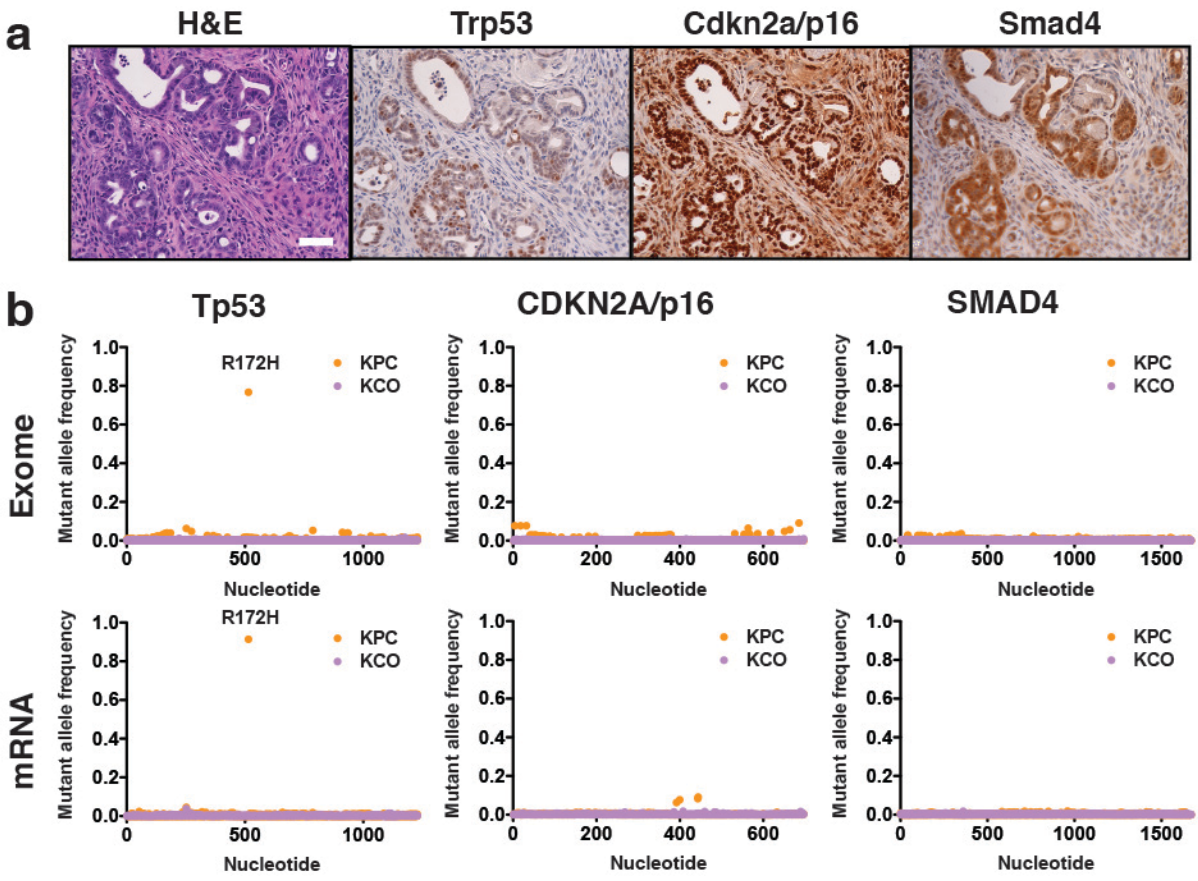

Supplementary Figure 3. Absence of PDAC driver alterations in *KCO* tumors.

a) Tumor suppressor genes frequently mutated in human cancers (*Trp53*, *Cdkn2A*/*p16*, and *Smad44*) were retained in *KCO* tumors as assessed by immunohistochemistry (IHC) and confirmed in 8/8 (100%) *KCO* tumors. Scale bar: 50 µm.

b) Exome and mRNA sequencing did not reveal new single nucleotide variants (SNVs) in *Trp53* (murine *p53* gene), *Cdkn2A/p16*, or *Smad4* in *KCO* tumors. Average mutant allele fraction identified for each base in the coding sequence of each tumor suppressor gene is shown for *KCO* mice. A single *KPC* tumor sequenced in parallel shows the presence of the expected R172H codon change and serves as a positive control for these analyses.

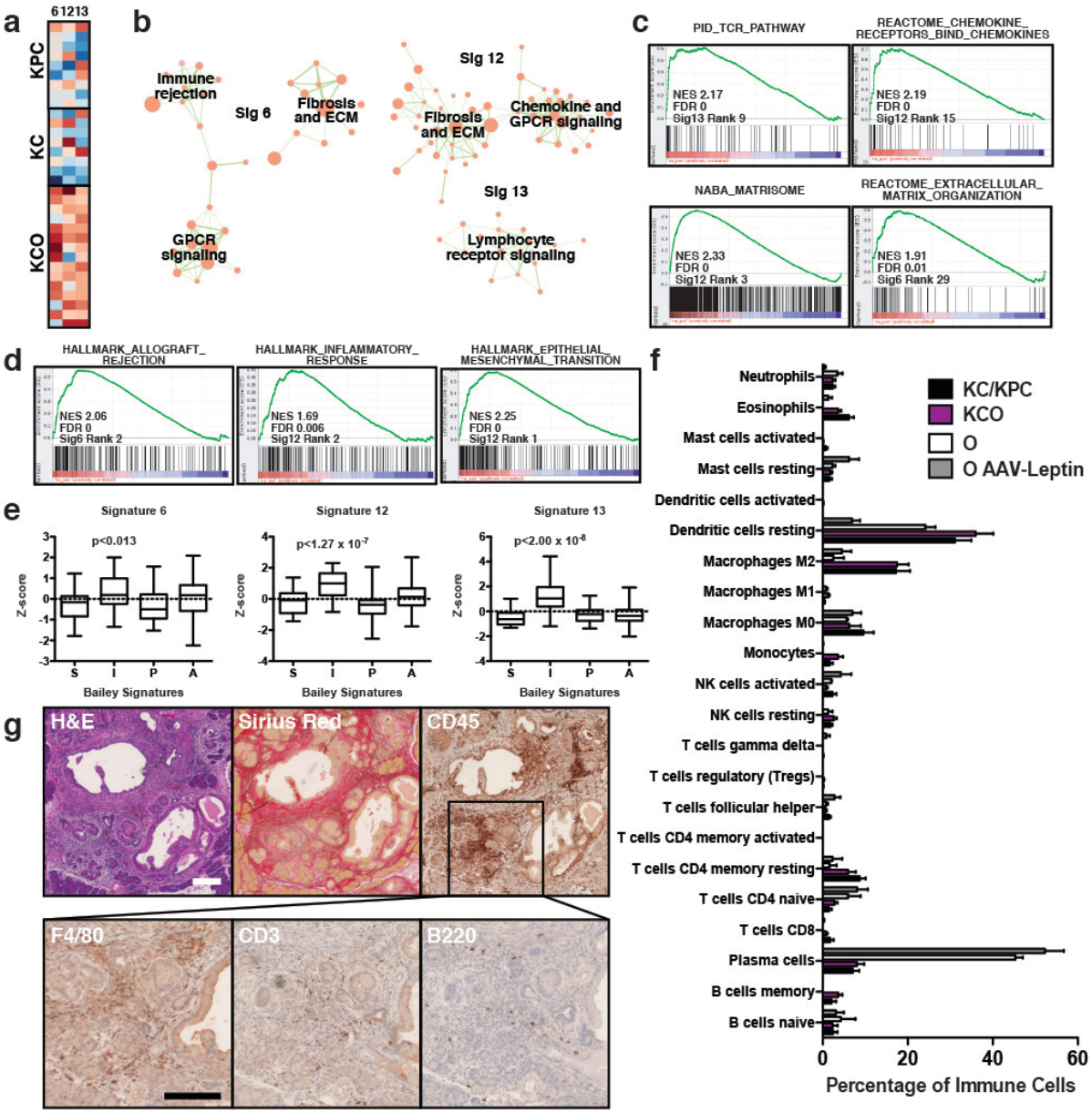

Supplementary Figure 4. Enhanced inflammation and fibrosis in *KCO* tumors.

a) Heat map of row normalized Z-scores (of mixing weights from the ICA decomposition) for ICA signatures (columns) showing statistically significant differences ($p<0.01$, Mann-Whitney test) between *KCO* mice versus non-obese *KC* and *KPC* mice. Signature numbers (6, 12, 13) are denoted above. Rows are individual tumors where the Z-score reflects relative correspondence between a tumor and the expression signature pattern (degree of positive or

negative correlation). Red corresponds to positive and blue to negative Z-scores.

b) Network representation of overlapping enriched GSEA/MSigDB gene sets associated with the signatures in (a). Cellular processes associated with related gene sets are listed.

c) GSEA using the curated gene set collection (C2 in MSigDB) revealed an association between *KCO* tumors and genes involved in immune cell activation/signaling and extracellular matrix (ECM)/fibrosis. Normalized enrichment score (NES), false discovery rate (FDR), ICA signature (*KCO* vs. *KC*/*KPC*), and MSigDB gene set rank (for C2 sets) used in analysis are shown. See **Supplementary Data Table 6** for complete list.

d) GSEA showed an association between *KCO* tumors and inflammation and fibrosis genes in comparison to hallmark genes set collection (H in MSigDB).

e) Box and whisker plots (boxes denote 25th-75th percentile, error bars denote min/max) of standardized signature scores of TCGA (scored using ssGSEA [67] for expression correlation with each of the signatures in (a) (6, 12, and 13) for each molecular subtype (S = squamous (n=31), I = immunogenic (n=28), P = progenitor (n=53), A = ADEX (n=38)). p-values confirmed significant enrichment of highly-correlated tumors with the immunogenic subtype (hypergeometric test) for each signature.

f) Immune cell proportions (average percentage of all immune cells +/- s.e.m.) based on CIBERSORT[35] of RNA-Seq data derived from non-obese tumor-bearing mice (*KC/KPC*, n=17), obese tumor-bearing mice (*KCO*, n=15), obese non-tumor-bearing mice (O: *ob/ob*, n=3), and non-obese non-tumor-bearing mice (*ob/ob* mice subject to AAV-Leptin, n=3).

g) Histologic analyses revealed extensive fibrosis (Sirius red staining of collagen) and CD45+ immune cell infiltration predominantly with F4/80+ macrophages and sparse presence of CD3+ T and B220+ B cells. Scale bars: 100 μm.

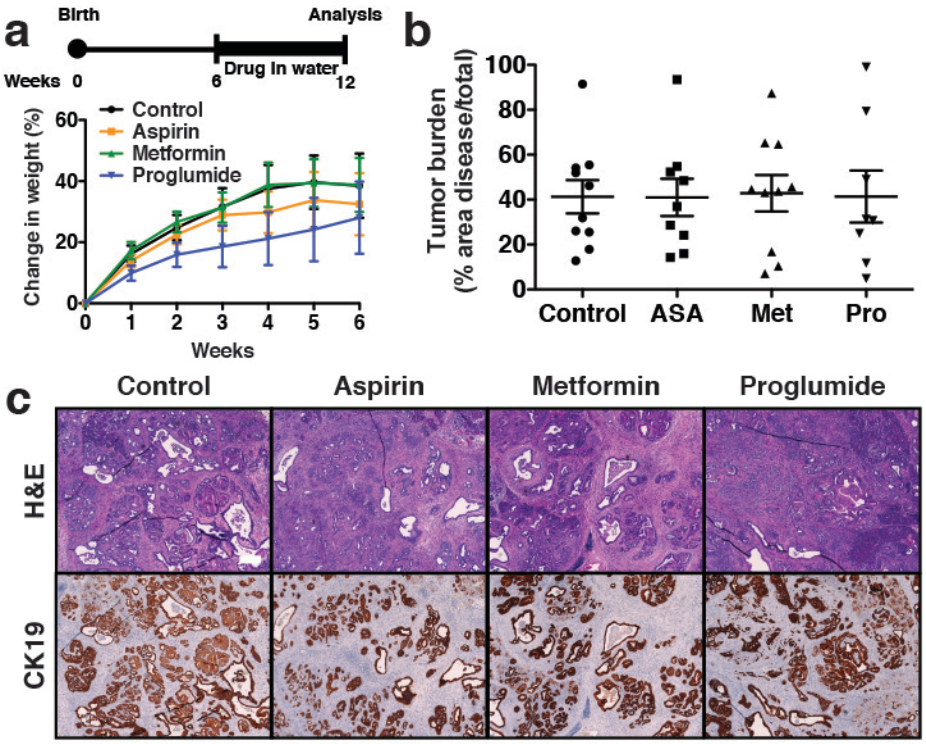

Supplementary Figure 5. Treatment studies in *KCO* mice.

a) Schematic shows treatment strategy in which mice are placed on drinking water containing drug at 6 weeks and analyzed for tumor progression 6 weeks later. Percent change in body weight (mean +/- s.e.m.) are shown for each treatment (n=7-10 mice/group). The CCK receptor antagonist proglumide showed a modest slowing of weight gain.

b) Quantification of tumor burden (average % cross-sectional area of disease/total +/- s.e.m.) is shown (n=7-10 mice/group) for each treatment (ASA = aspirin, Met = metformin, Pro = proglumide) and control drinking water. No significant differences were observed ($p>0.05$, two-tailed student's t-test).

c) Representative histologic sections of pancreata of mice at endpoint demonstrate comparable development of CK19-positive ductal tumors in all treatment groups in (b). Scale bar: 200 μm.

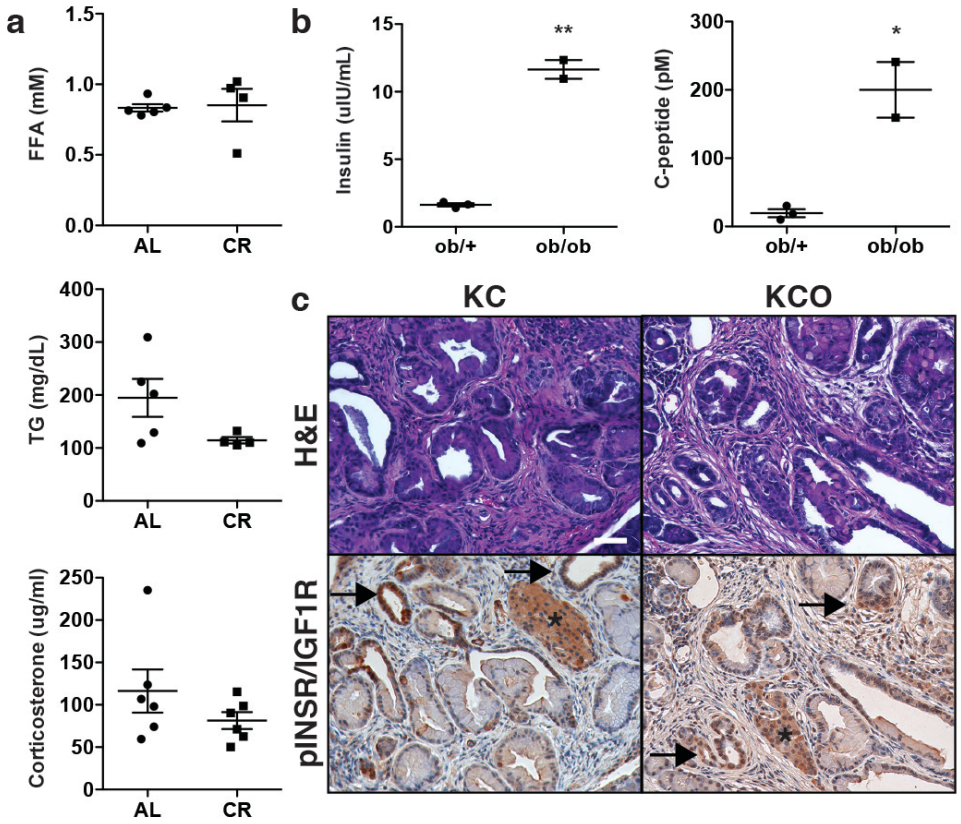

Supplementary Figure 6. Insulin signaling but not changes in circulating lipids or glucocorticoids influence pancreatic tumorigenesis.

a) Non-fasting serum free fatty acids (FFA), triglycerides (TG), and corticosterone levels did not significantly change (p>0.05, two-tailed student's t-test,) in *KCO* mice subject to caloric restriction compared to ad libitum mice (n=4-6 mice/group).

b) Obese leptin-deficient (*ob/ob)* mice exhibited increased fasting serum insulin and C-peptide levels compared to non-obese controls (*ob/+*) at 10 weeks (n=2-3 mice/group). *p<0.05, **p<0.01, two-tailed student's t-test.

c) IHC reveals activated insulin receptor/Igf1 receptor (phospho-InsR/Igf1R) in PanINs in non-obese (*KC*) and obese (*KCO*) mice, consistent with insulin-induced signaling. pInsR/Igf1R increases in higher-grade PanINs (arrows). Pancreatic islets were internal positive controls (asterisk). Scale bar: 50 µm.

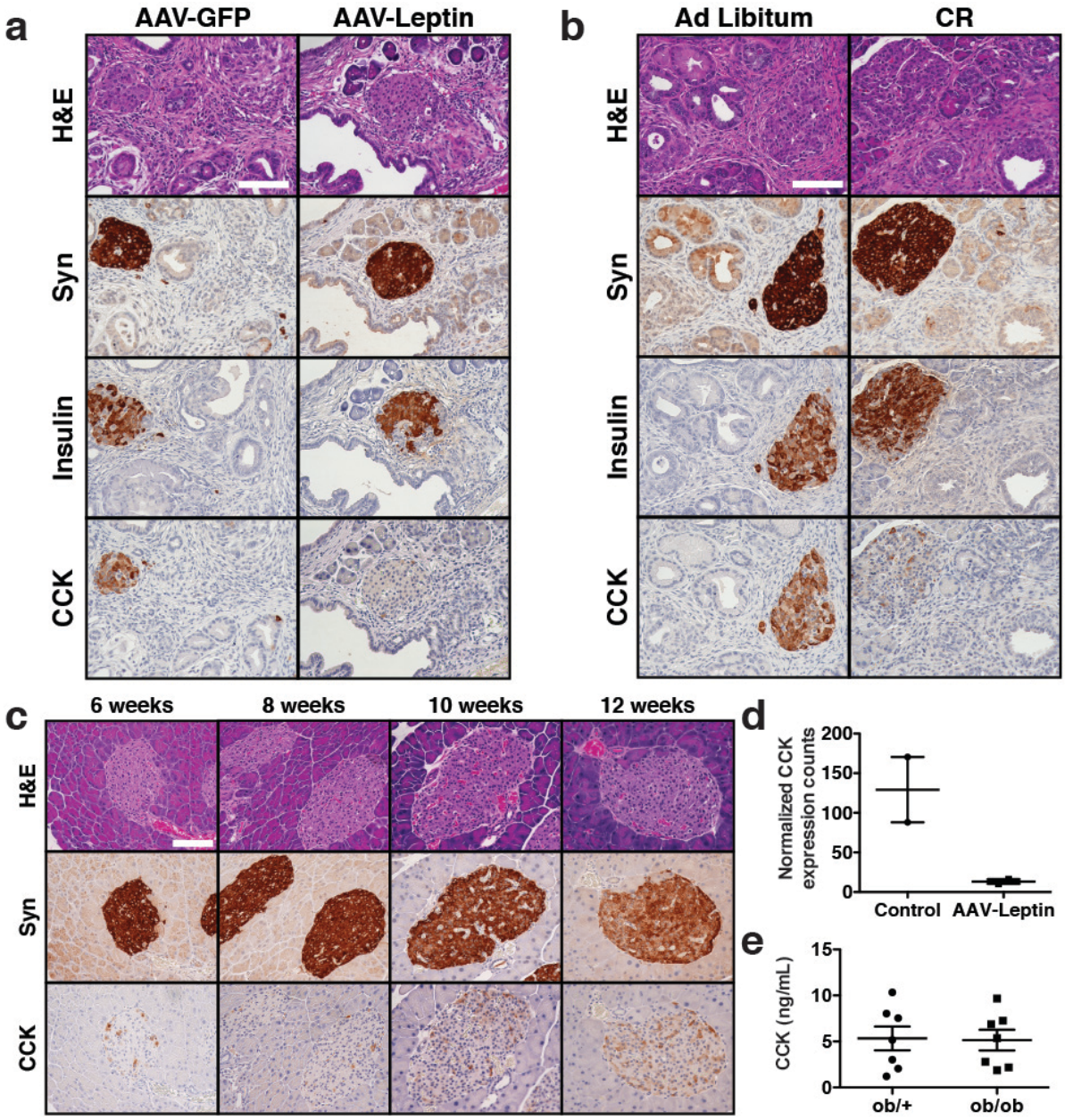

Supplementary Figure 7. Obesity-associated islet CCK expression in mice.

a) Islet CCK expression is abolished following AAV-Leptin treatment of *KCO* mice. Synaptophysin (Syn) designates islets and insulin denotes beta cells. Mice were analyzed at 12 weeks of age following intervention starting at 6 weeks of age. Scale bar: 100 µm.

b) Islet CCK expression was markedly reduced following weight loss induced by caloric restriction in *KCO* mice. Scale bar: 100 µm.

c) Obese (*ob/ob*) mice exhibit progressive expression of CCK in pancreatic islets in the absence of tumors development. Scale bar: 100 μm.

d) AAV-leptin treatment of *ob/ob* mice reduced CCK expression by RNA-Seq on bulk pancreata. Normalized CCK expression counts +/- s.e.m. are shown (n=2 mice/group).

e) Non-fasting serum CCK levels did not differ between 7-9 week-old obese *ob/ob* and non-obese *ob/+* mice (n=7 mice/group).

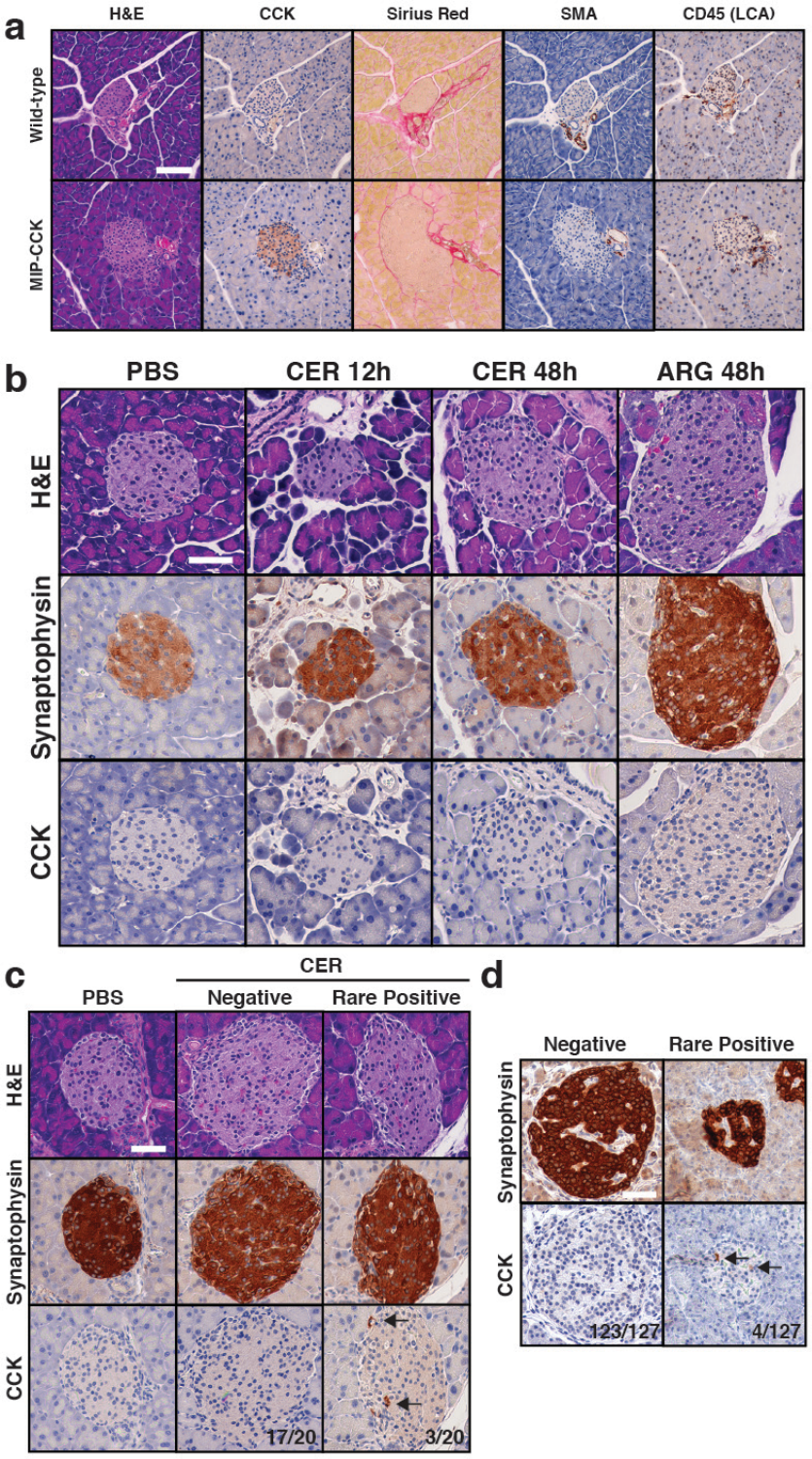

Supplementary Figure 8. Disconnect between islet CCK expression and pancreatic inflammation.

a) *MIP-CCK* transgenic mice exhibited islet-specific CCK expression without evidence of

pancreatic inflammation (CD45-positive leukocyte infiltration) or fibrosis (Sirius red collagen staining or presence of smooth muscle actin (SMA)-positive fibroblasts compared to wild-type controls. Scale bar: 100 µm.

b) CCK is not significantly expressed in pancreatic islets in murine models of acute pancreatitis (CER = cerulein, ARG = arginine, PBS is control). Scale bar: 100 µm.

c) CCK is rarely expressed (arrows) in pancreatic islets in a murine model of chronic pancreatitis (cerulein-treated for 2 weeks). Frequencies of islets without staining (negative) or rare CCK-positive cells (arrows) are shown. Scale bar: 100 µm.

d) CCK is rarely expressed (arrows)in pancreatic islets obtained from patients with chronic pancreatitis. Frequencies of islets without staining (negative) or rare CCK-positive cells are shown. Scale bar: 100 µm.

Patient characteristic	Mean (SD)
Age at surgery, years	65.5 (10.7)
BMI (kg/m^2)	26.7 (5.2)
Overall survival (months)	23.1 (19.2)
Disease free survival (months)	15.4 (17.2)
Tumor size (cm)	3.6 (1.4)
Sex	**N (%)**
Men	113 (61)
Women	71 (39)
Race	**N (%)**
White	144 (78)
Black	24 (13)
Other/missing	16 (9)
Study site	**N (%)**
DFCI/BWH[1]	12 (7)
URMC[2]	70 (38)
SCI[3]	102 (55)
Tumor location	**N (%)**
Head/uncinate	138 (75)
Body	18 (10)
Tail	25 (14)
Unknown	3 (2)
N stage	**N (%)**
N0	55 (30)
N1	128 (70)
NX	1 (1)

[1]Dana-Farber Cancer Institute/Brigham and Women's Hospital
[2]University of Rochester Medical Center
[3]Stanford Cancer Institute

Supplementary Table 1. Characteristics of patients with available body mass index (BMI) and molecular alterations data.

BMI	WT	*KRAS* MUT	OR (95% CI)[1]
<25 kg/m^2	5 (7)	71 (93)	Ref
25-30 kg/m^2	4 (7)	57 (93)	1.15 (0.29-4.67)
>30 kg/m^2	4 (9)	43 (91)	0.86 (0.21-3.60)
BMI	**WT**	***TP53* MUT**	**OR (95% CI)[1]**
<25 kg/m^2	30 (39)	46 (61)	Ref
25-30 kg/m^2	19 (31)	42 (69)	1.38 (0.66-2.85)
>30 kg/m^2	14 (30)	33 (70)	1.41 (0.63-3.13)
BMI	**WT**	***CDKN2A/p16* MUT**	**OR (95% CI)[1]**
<25 kg/m^2	19 (25)	57 (75)	Ref
25-30 kg/m^2	16 (26)	45 (74)	1.22 (0.54-2.76)
>30 kg/m^2	13 (28)	34 (72)	1.16 (0.48-2.80)
BMI	**WT**	***SMAD4* MUT**	**OR (95% CI)[1]**
<25 kg/m^2	43 (57)	33 (43)	Ref
25-30 kg/m^2	34 (56)	27 (44)	1.16 (0.58-2.34)
>30 kg/m^2	**14 (30)**	**33 (70)**	**3.82 (1.69-8.66)**
BMI	**N patients**	**PDAC Drivers[2] # of mutations**	**p-value[3]**
<25 kg/m^2	76	2.7 (0.9)	0.19
25-30 kg/m^2	61	2.8 (0.9)	
>30 kg/m^2	47	3.0 (0.9)	

[1]Adjusted for age at surgery, study site, and gender
[2]*KRAS*, *TP53*, *CDKN2A*, *SMAD4* exome mutation or loss by IHC
[3]Kruskal-Wallis test

Supplementary Table 2. Association of BMI with PDAC driver gene alterations in human tumors.

Number (percentage of patients) at each BMI level are shown for each gene. For number of mutations, mean (standard deviation) is shown for each BMI level.

SUPPLEMENTARY DATA TABLES

Supplementary Data Table 1. Tumor suppressor gene (TSG) single nucleotide variants (SNVs) in *KCO* tumors.

Mutant allele fractions for each coding nucleotide (compared to mm9 reference database) of tumor suppressor genes (*Trp53*, *CDKN2A/p16*, and *SMAD4*) derived from whole exome sequencing and RNA-Seq are shown for individual *KCO* tumors and averaged across all tumors Average base coverage across *KCO* tumors are as follows: *Trp53* (84X exome, 127X RNA), *CDKN2A/p16* (40X exome, 89X RNA), and *SMAD4* (103X exome, 86X RNA). Blank cells denote lack of base coverage in sequencing, which was rare and sporadic. A single *KPC* tumor (7075) was used as a positive control for SNV detection (resulting in a R172H codon substitution as noted). No tumor suppressor gene SNVs were detected in *KCO* tumors.

Supplementary Data Table 2. Single nucleotide variants in murine tumors.

All single nucleotide variants (SNV) called in *KCO* (n=13) and *KPC* (n=1) tumors by whole exome sequencing are listed by tumor. Variant information includes location (chromosome, cytoband, and position in mm9 genome), genic location (exonic, intergenic, UTR), nucleotide change (var vs. ref), read counts for variant (tumor_reads2) and reference (tumor_reads1), and variant frequency (tumor_var_freq). Exon SNVs were further classified as synonymous or non-synonymous with reference to transcript (RefSeq), exon number (Exon_num), and coding sequence position (AA_change).

Supplementary Data Table 3. Compilation of non-synonymous single nucleotide variants in murine tumors.

Compiled non-synonymous single nucleotide variants (SNVs) identified on whole exome sequencing data derived from all sequenced *KCO* and *KPC* tumors from **Supplementary Data Table 2**. A total of 531 SNVs were called from 14 tumors (~37.7 SNVs per *KCO* mouse (n=13) and 41 SNVs in *KPC* mouse (n=1)). Induced *Kras*, *Lep* (*ob*), and *Trp53* mutations were observed as expected. Of consensus pan-cancer genetic drivers[32], *Arid5b, Cacna1a, Eef2*, and *Kit* harbored recurrent non-synonymous SNVs. These SNVs were not observed in human cancer (COSMIC) to suggest pathogenicity.

Supplementary Data Table 4. Normalized expression counts for RNA-Seq of tumors.

Log (base 2) transformed normalized expression counts per gene in individual *KCO*, *KC*, and *KPC* tumors used in RNA-Seq analyses. Mouse number, genotype, and AAV treatments are shown.

Supplementary Data Table 5. *KCO*-related gene signatures derived by independent component analysis (ICA).

Gene signatures that distinguish obese (*KCO*) and non-obese (*KC* and *KPC*) tumors by ICA with $p<0.05$ are shown. Per-gene expression correlation Z-scores with respect to the signature are listed (positive is correlated with *KCO* tumors) for each gene signature and ordered by log2 fold change comparing above groups.

Supplementary Data Table 6. Gene set enrichment analyses (GSEA) to determine *KCO*-related pathways.

GSEA results correlated with *KCO* tumors (UP) are shown comparing ICA-derived signatures (6, 12, and 13) in **Supplementary Data Table 5** with curated (C2) and hallmark (H) gene sets in MSigDB.